Supporting Materials

In situ studies of reversible solid-gas reactions of ethylene responsive silver pyrazolates

H. V. Rasika Dias,[1,*] Devaborniny Parasar,[1] Andrey A. Yakovenko,[2,*] Peter W. Stephens,[3,*] Álvaro R. Muñoz-Castro,[4,*] Mukundam Vanga,[1] Pavel Mykhailiuk,[5,6] Evgeniy Slobodyanyuk[5]

[1] Department of Chemistry and Biochemistry, The University of Texas at Arlington, Arlington, Texas 76019, USA; [2] X-Ray Science Division, Advanced Photon Source, Argonne National Laboratory, Argonne, Illinois 60439, USA; [3] Department of Physics and Astronomy, Stony Brook University, Stony Brook, NY 11794-3800, USA; [4] Facultad de Ingeniería, Arquitectura y Diseño, Universidad San Sebastián, Bellavista 7, Santiago, 8420524, Chile; [5] Enamine Ltd., Chervonotkatska 78, 02094 Kyiv, Ukraine; [6] Taras Shevchenko National University of Kyiv, Faculty of Chemistry; Volodymyrska 60, 01601 Kyiv, Ukraine

Synthesis and characterization of {[3,4,5-$(CF_3)_3$Pz]Ag}$_3$ ([Ag-CF_3]$_3$) and {[3,4,5-$(CF_3)_3$Pz]Ag(C_2H_4)}$_2$ ([Ag-CF_3•(C_2H_4)]$_2$)

General Information

All manipulations were carried out under an atmosphere of purified nitrogen using standard Schlenk techniques or in a MBraun glovebox equipped with a -25 °C refrigerator. Solvents were purchased from commercial sources and purified before use. NMR spectra were recorded at 25 °C on a JEOL Eclipse 500 spectrometer (^{1}H, 500.16 MHz ^{13}C, 125.78 MHz, and ^{19}F, 470.62 MHz) unless otherwise noted. ^{1}H and ^{13}C NMR spectra are referenced to the solvent peak (^{1}H; $CDCl_3$ δ 7.26, ^{13}C; $CDCl_3$ δ 77.16). ^{1}H NMR coupling constants (J) are reported in Hertz (Hz) and multiplicities are indicated as follows: s (singlet), d (doublet), t (triplet), m (multiplet). ^{19}F NMR values were referenced to external $CFCl_3$. Melting points were obtained on a Mel-Temp II apparatus and were not corrected. Elemental analyses were performed using a Perkin-Elmer Model 2400 CHN analyzer. IR spectra were collected at room temperature on a Shimadzu IR Prestige-21 FTIR containing an ATR attachment using pure liquid or solid materials, with instrument resolution at 2 cm^{-1}. Raman data were collected on a Horiba Jobin Yvon LabRAM Aramin Raman spectrometer with a HeNe laser source of 633 nm, by placing pure solid materials on a glass slide. All other reactants and reagents were purchased from commercial sources. Heating was accomplished by either a heating mantle or a silicone oil bath. The 3,4,5-$(CF_3)_3$PzH[1] was prepared via reported methods.

Synthesis of {[3,4,5-$(CF_3)_3$Pz]Ag}$_3$ ([Ag-CF_3]$_3$)

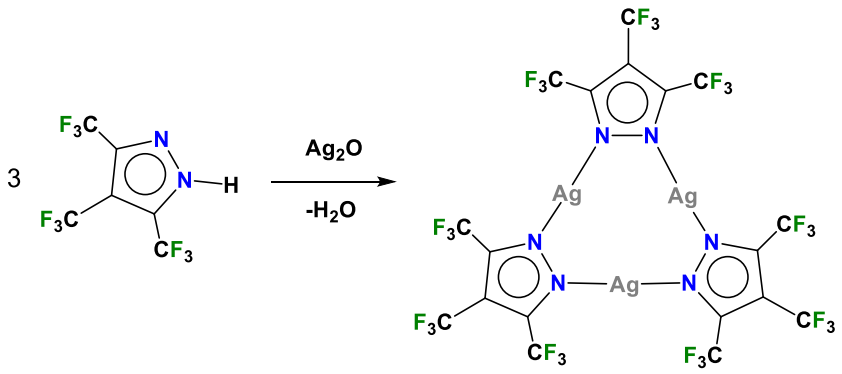

Freshly dried 3,4,5-$(CF_3)_3$PzH (300 mg, 1.10 mmol) and Ag_2O (211 mg, 0.91 mmol) were placed in a Schlenk flask attached to a reflux condenser, slowly heated to 125-130 °C and kept for 4 h while stirring, or until unreacted pyrazole stops condensing on the walls the flask. A heat gun was used to meltdown the pyrazole condensed on the wall of the Schlenk flask, as needed. Excess 3,4,5-$(CF_3)_3$PzH was sublimated off, the product was extracted into dichloromethane, and filtered through a bed of Celite. The filtrate was collected, and solvent was removed under reduced pressure to obtain {[3,4,5-$(CF_3)_3$Pz]Ag}$_3$ (**[Ag-CF_3]$_3$**) as a white powder. X-ray quality crystals were grown from dichloromethane at -20 °C. Yield: 91%. M.p.: 260 °C. Anal. Calc. for $C_{18}N_6F_{27}Ag_3$: C, 19.02; H, 0.00; N, 7.39. Found: C, 18.98; H, <0.1; N, 7.41. ^{19}F NMR (in $CDCl_3$): δ (ppm) -54.94 (br s), -60.63 (q, 7.2 Hz). $^{13}C\{^1H\}$ NMR (in $CDCl_3$): δ (ppm) 110.6 (q, $^2J(C,F)$ = 42.0 Hz, *C*CF_3), 119.2 (q, $^1J(C,F)$ = 270.3 Hz, *C*F_3), 120.7 (q, $^1J(C,F)$ = 262.7 Hz, *C*F_3), 143.5 (q, $^2J(C,F)$ = 36.0 Hz, *C*CF_3). Raman (cm^{-1}): 3148, 1594, 1536, 1502, 1453, 1349, 1154, 1088, 1000, 985, 845.

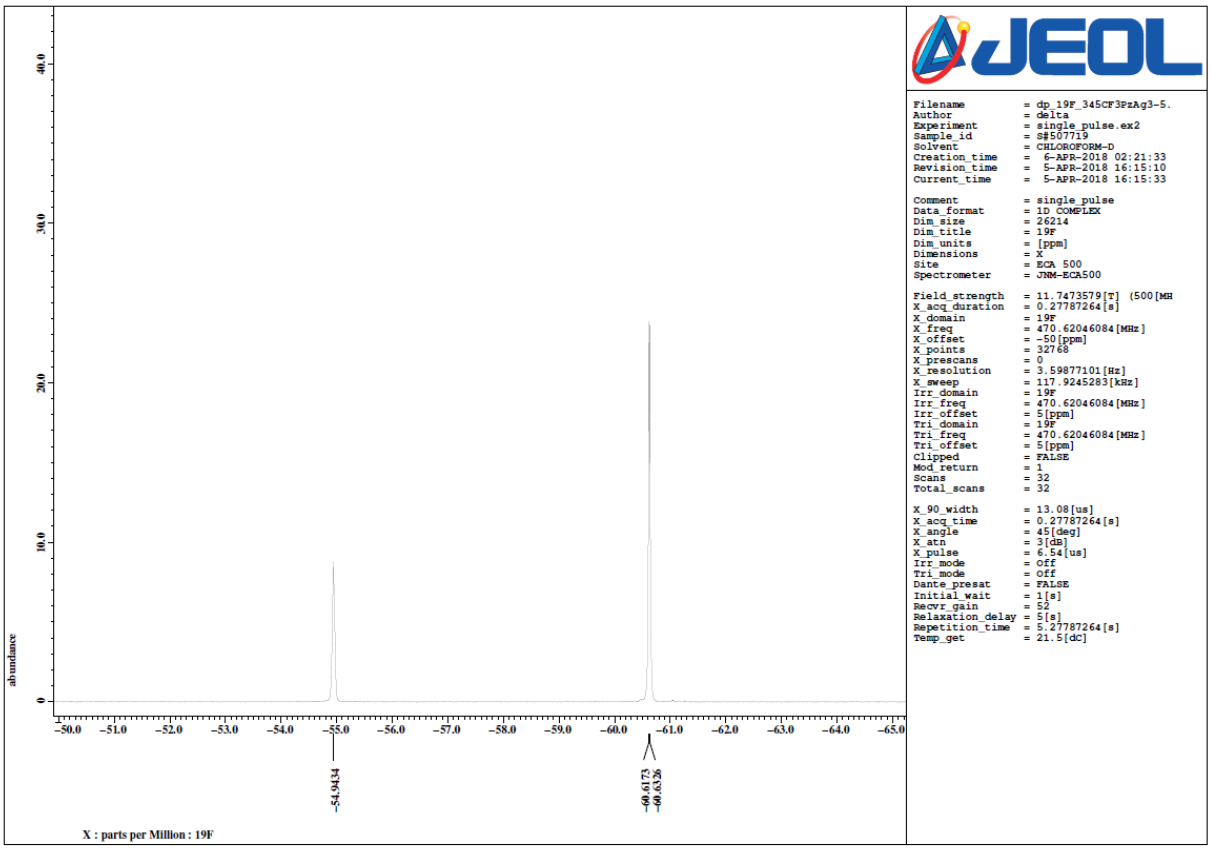

Figure S1. ^{19}F NMR spectrum of **{[3,4,5-(CF_3)$_3$Pz]Ag}$_3$** in $CDCl_3$ at the room temperature.

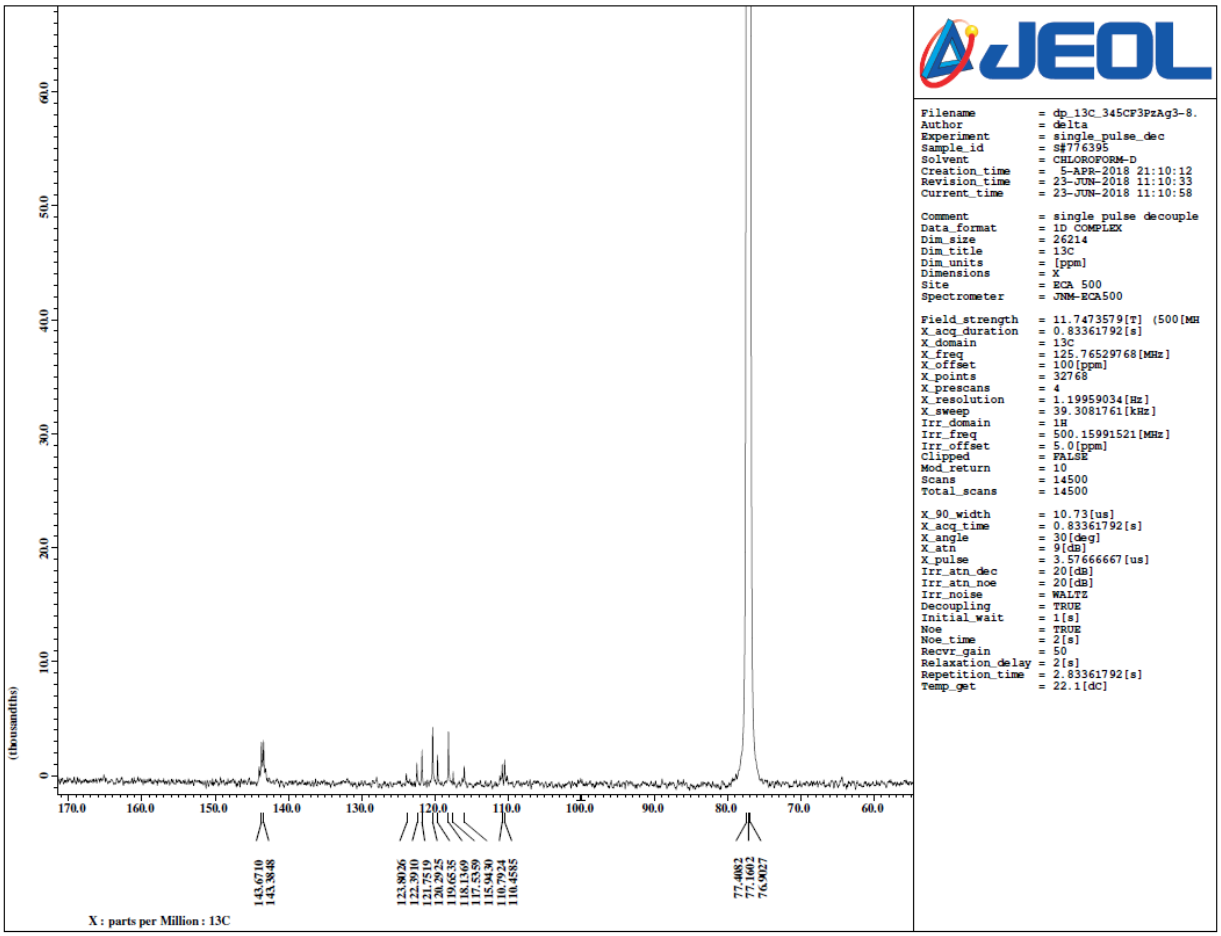

Figure S2. $^{13}C\{^{1}H\}$ NMR spectrum of **{[3,4,5-(CF$_3$)$_3$Pz]Ag}$_3$** in $CDCl_3$ at the room temperature.

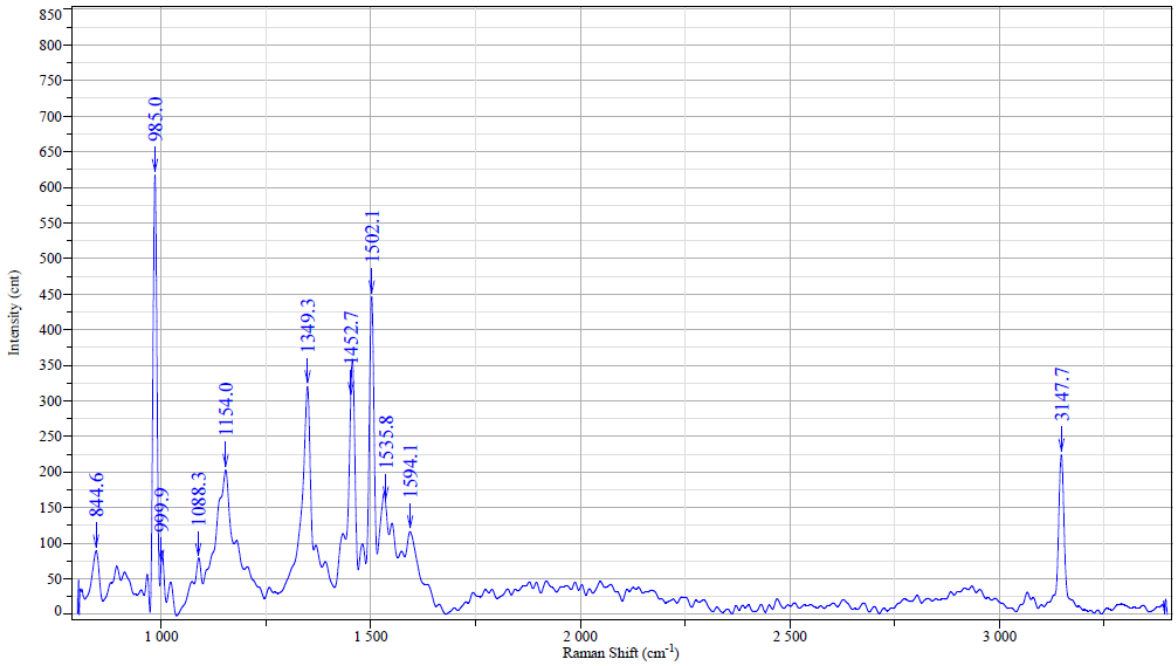

Exposition	5	Slit	100
Accumulation	5 x 4	Operator	Parasar
Laser	632.817	Sample	Ag3
Spectro	Multi	Remark	
Hole	200	Power	

HORIBA JOBIN YVON

Figure S3. Raman spectrum of **{[3,4,5-(CF$_3$)$_3$Pz]Ag}$_3$**

Synthesis of {[3,4,5-$(CF_3)_3Pz$]Ag(C_2H_4)}$_2$

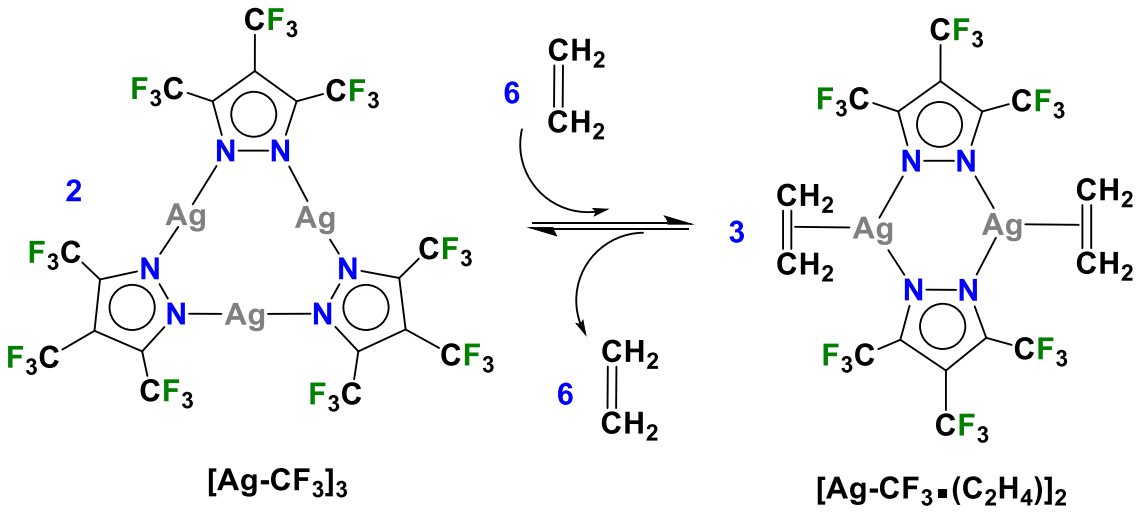

{[3,4,5-$(CF_3)_3Pz$]Ag}$_3$ (200 mg, 0.18 mmol) was dissolved in 10-12 mL of CH_2Cl_2, ethylene was bubbled for ~10 min. The ethylene saturated solution was kept at -25 °C to obtain X-ray quality colorless crystals of {[3,4,5-$(CF_3)_3Pz$]Ag(C_2H_4)}$_2$ (**[Ag-CF_3•(C_2H_4)]$_2$**). Yield: 96%. ^{19}F NMR (in $CDCl_3$ at -50°C): δ (ppm) -60.00 (3,5-CF_3) and -54.97 (4-CF_3). ^{1}H NMR (in $CDCl_3$ at -50°C): δ (ppm) 5.42.

NMR Studies of solution-state equilibria for the [Ag-CF_3•(C_2H_4)]$_2$ reaction with ethylene

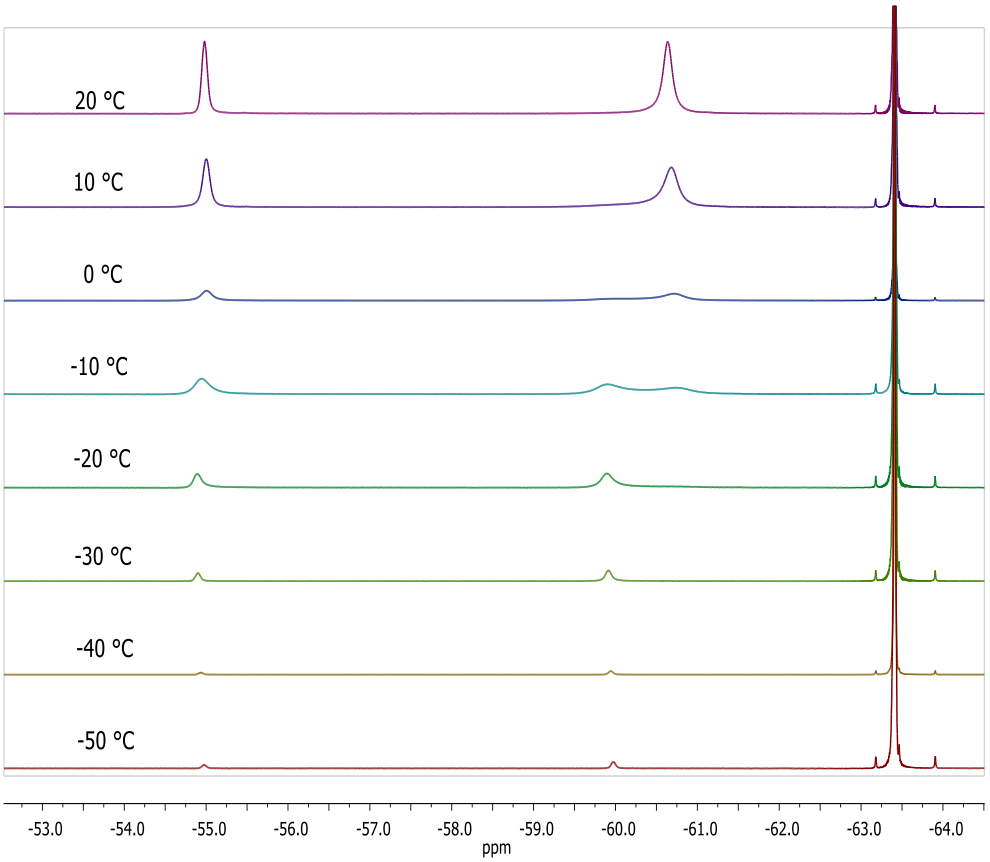

Figure S4. ^{19}F NMR spectra of **[Ag-CF_3•(C_2H_4)]$_2$/[Ag-CF_3]$_3$**/ethylene at various temperatures. (Referenced to internal standard at constant value, 1,3,5-$(CF_3)_3C_6H_3$ was used as the internal standard (-63.41 ppm)). The data were collected using crystalline **[Ag-CF_3•(C_2H_4)]$_2$.**

As evident from these spectra, at 20 °C in $CDCl_3$, **[Ag-CF_3•(C_2H_4)]$_2$** completely dissociates into **[Ag-CF_3]$_3$** and free ethylene. Therefore, ^{19}F NMR peaks corresponding to **[Ag-CF_3]$_3$** species can be observed at 20 °C (-60.64 and -54.98 for 3,5-CF_3 and 4-CF_3, respectively).

From 0°C to -20 °C signals for both **[Ag-CF_3•(C_2H_4)]$_2$** and **[Ag-CF_3]$_3$** was observed in various ratios.

From -30 °C to -50 °C only signals corresponding to **[Ag-CF_3•(C_2H_4)]$_2$** is observed (-60.00 and -54.97 ppm corresponding to 3,5-CF_3 and 4-CF_3 groups, respectively).

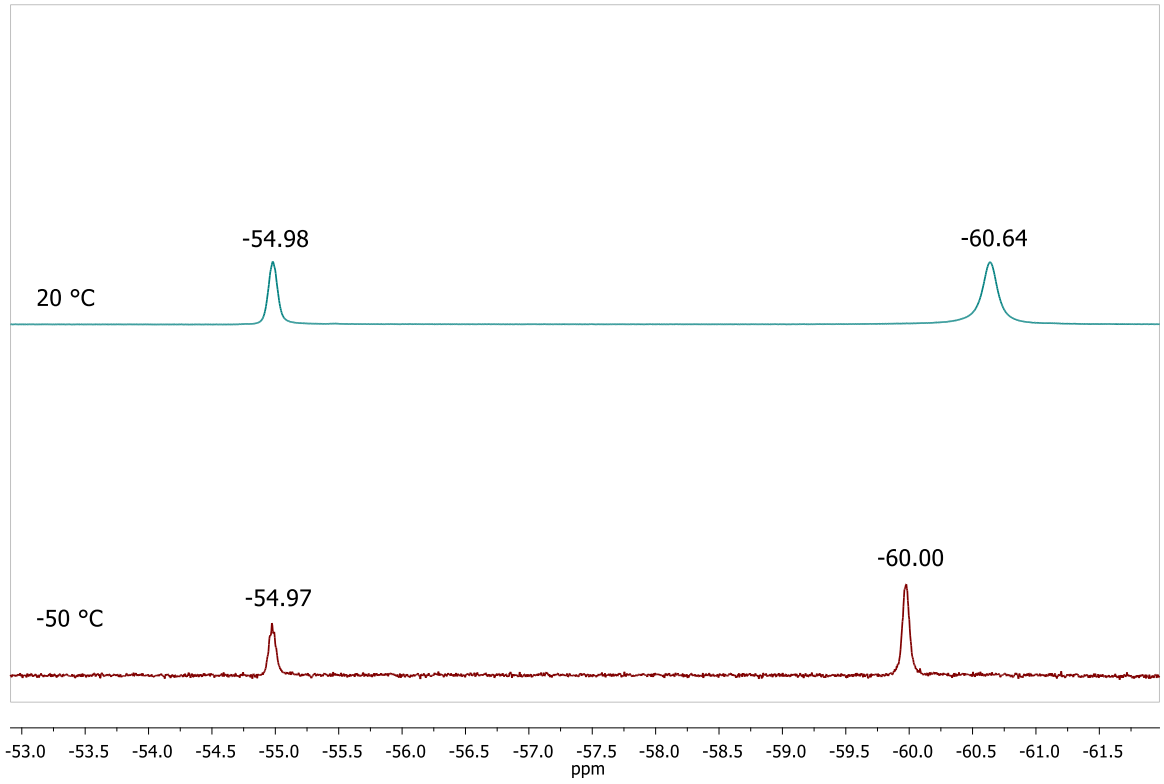

Figure S5. Another view ^{19}F NMR spectra of **[Ag-CF_3•(C_2H_4)]$_2$/[Ag-CF_3]$_3$**/ethylene mixture at 20 °C (exclusively **[Ag-CF_3]$_3$** and free ethylene) and -50 °C (**[Ag-CF_3•(C_2H_4)]$_2$**).

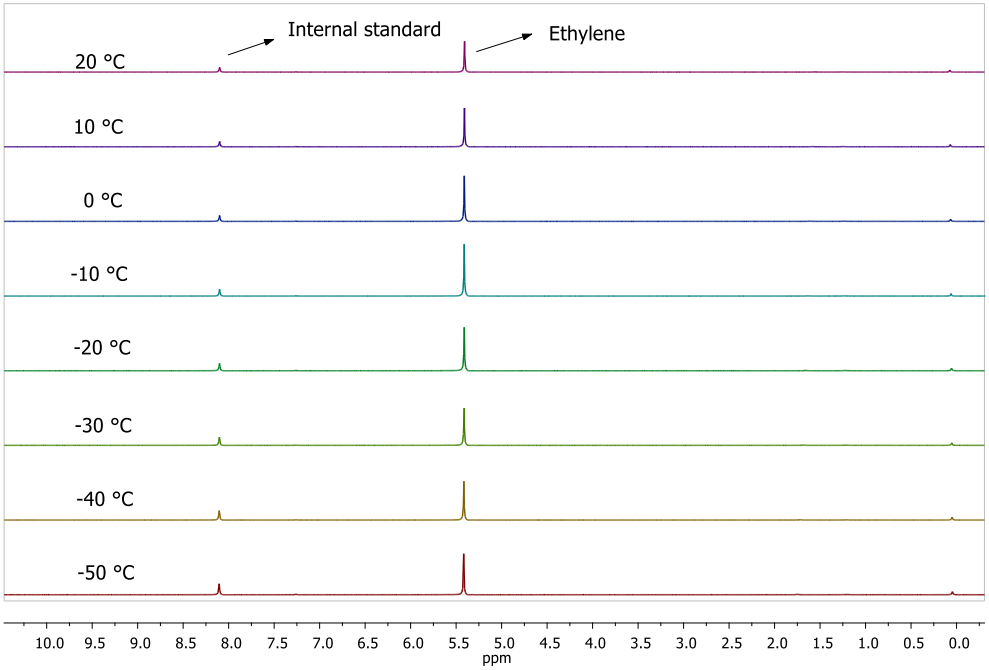

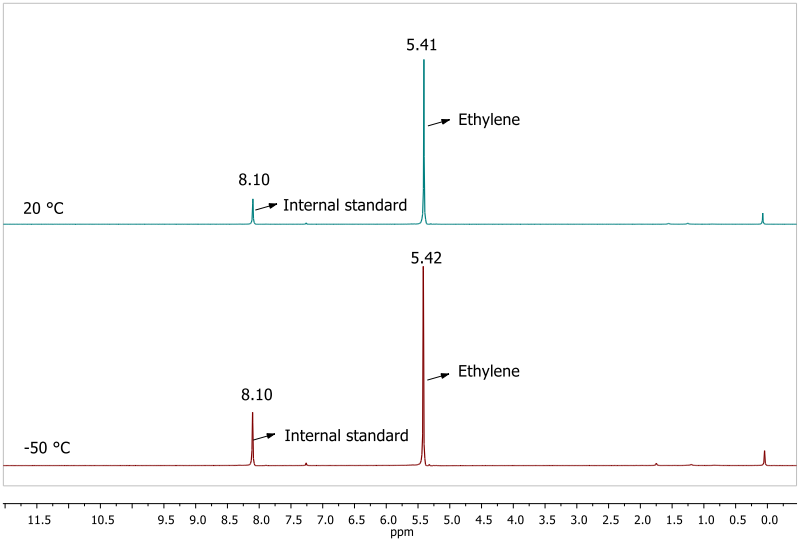

Figure S6; ^{1}H NMR spectra (two views) of NMR spectra of **[Ag-CF$_3$•(C$_2$H$_4$)]$_2$/[Ag-CF$_3$]$_3$**/ethylene at various temperatures.

No clear shift is observable perhaps due to highly fluxional Ag-ethylene interaction although the ^{19}F NMR data indicated the formation of **[Ag-CF$_3$•(C$_2$H$_4$)]$_2$** from **[Ag-CF$_3$]$_3$**/ethylene when the temperature is lower than -10 °C.

Single crystal X-ray crystallography.

A suitable crystal covered with a layer of hydrocarbon/Paratone-N oil was selected and mounted on a Cryo-loop, and immediately placed in the low-temperature nitrogen stream. The X-ray intensity data were measured at 100(2) K on a Bruker D8 Quest with a Photon 100 CMOS detector equipped with an Oxford Cryosystems 700 series cooler, a graphite monochromator, and a Mo Kα fine-focus sealed tube (λ = 0.71073 Å). Intensity data were processed using the Bruker Apex program suite. Absorption corrections were applied by using SADABS.[2] Initial atomic positions were located by SHELXT,[3] and the structures of the compounds were refined by the least-squares method using SHELXL[4] within Olex2 GUI.[5] All the non-hydrogen atoms were refined anisotropically. There are two molecules of **[Ag-CF_3•(C_2H_4)]$_2$** in the asymmetric unit. It was solved and refined in $Pna2_1$ space group as an inversion twin. We have also tested the possibility of Pccn space group for **[Ag-CF_3•(C_2H_4)]$_2$** suggested by the CheckCif but the refinement indicators were significantly poor. The hydrogen atoms of the ethylene groups of **[Ag-CF_3•(C_2H_4)]$_2$** were located using difference Fourier maps, included, and refined freely with isotropic displacement parameters. The hydrogen atoms of **[Ag-CF_3]$_3$**•CH_2Cl_2 were included in their calculated positions and refined as riding on the atoms to which they are joined. X-ray structural figures were generated using Olex2.[5] The **CCDC** 2256899-2256900 files contain the supplementary crystallographic data for **[Ag-CF_3]$_3$**•CH_2Cl_2 and **[Ag-CF_3•(C_2H_4)]$_2$**. These data can be obtained free of charge via http://www.ccdc.cam.ac.uk/conts/retrieving.html or from the Cambridge Crystallographic Data Centre (CCDC), 12 Union Road, Cambridge, CB2 1EZ, UK).

Single crystal X-ray crystallography of [Ag-CF_3]$_3$•CH_2Cl_2

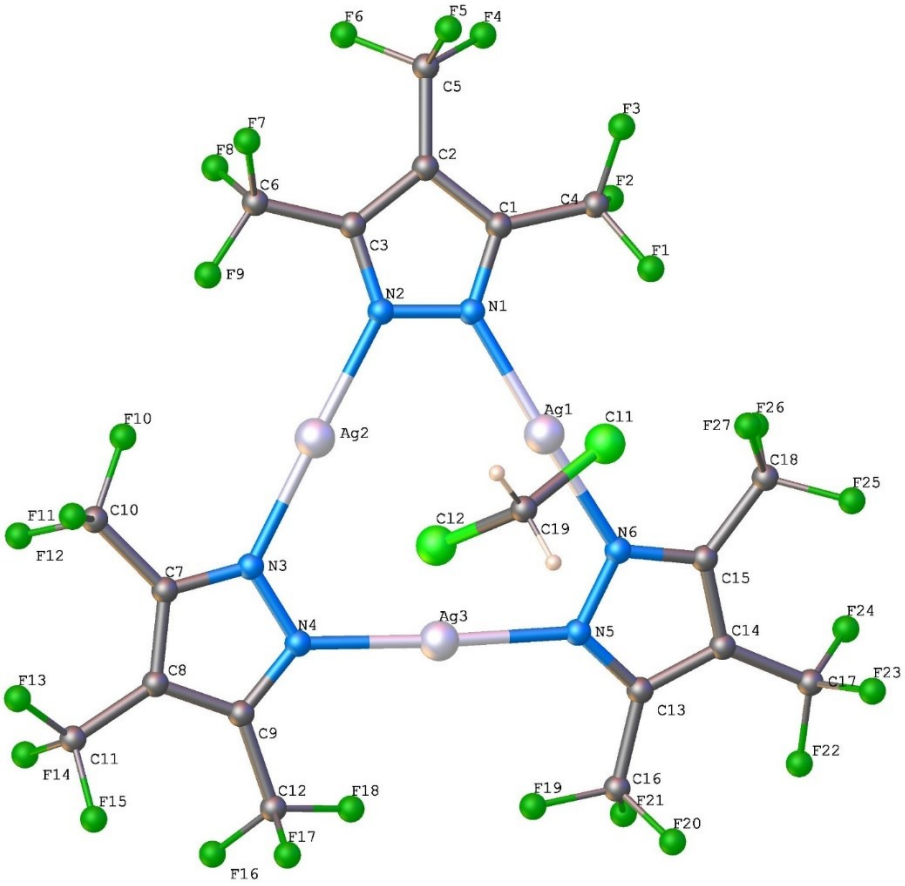

Figure S7. Molecular structure and atom labelling scheme of **[Ag-CF_3]$_3$•CH_2Cl_2**

The analysis of the crystal of **[Ag-CF_3]$_3$** obtained from dichloromethane by single crystal X-ray diffraction show that it crystallizes as **[Ag-CF_3]$_3$•CH_2Cl_2** from dichloromethane in $P\bar{1}$ space group with chlorine atoms facing silver sites (Figure S8), with Ag-Cl contacts shorter than the van der Waals contact separation of Ag and Cl (3.47 Å). This suggest that the silver sites are quite Lewis acidic even to interact with weakly donating CH_2Cl_2 which is not surprising considering the number of electron-withdrawing fluorinated substituents on the ligand backbone. The solvent molecules in the crystal lattice, however, can be removed easily under reduced pressure to obtain **[Ag-CF_3]$_3$**, of which structure was confirmed by analyzing the material using powder X-ray diffraction (Figure S14 below).

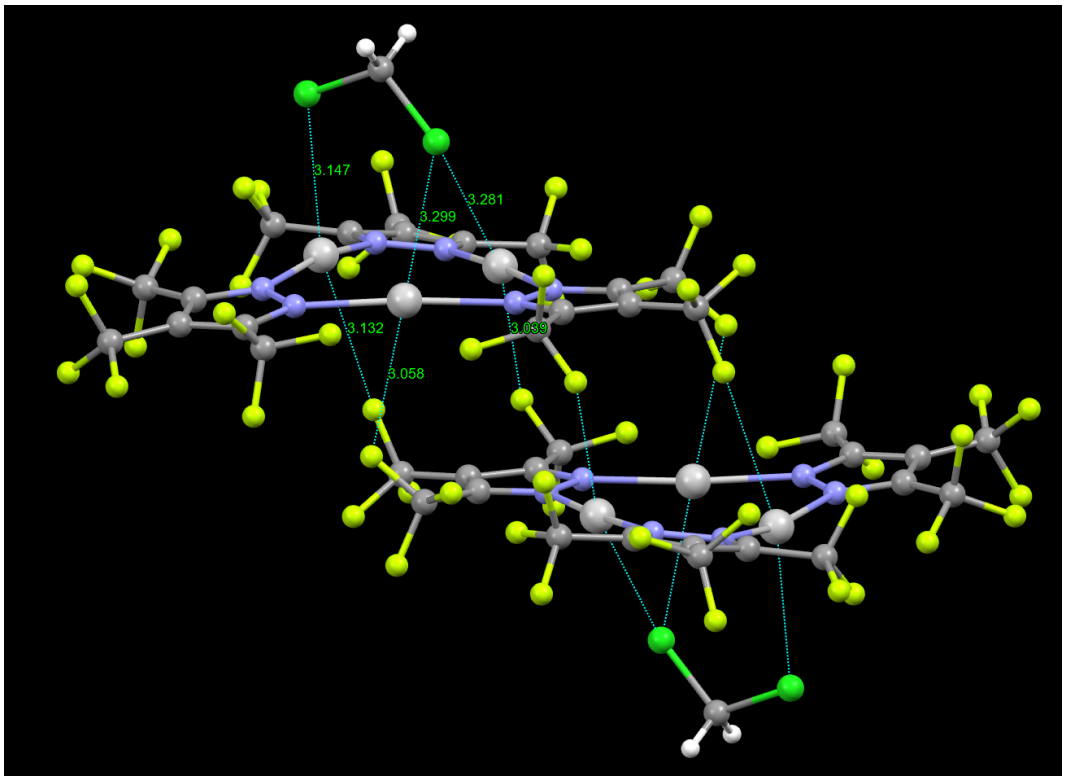

Figure S8. Single crystal X-ray structure of **[Ag-CF_3]$_3$**•CH_2Cl_2 showing Ag···Cl and Ag···F interactions.

Table S1. Crystal data and structure refinement for **[Ag-CF_3]$_3$•CH_2Cl_2**.

Identification code	Rad629
Empirical formula	$C_{19}H_2Ag_3Cl_2F_{27}N_6$
Formula weight	1221.78
Temperature/K	100
Crystal system	triclinic
Space group	P-1
a/Å	9.4750(8)
b/Å	10.5097(9)
c/Å	18.0959(16)
α/°	95.547(2)
β/°	98.944(2)
γ/°	116.476(2)
Volume/Å^3	1565.1(2)
Z	2
ρ_{calc}g/cm^3	2.593
μ/mm^{-1}	2.219
F(000)	1152.0
Crystal size/mm^3	0.38 × 0.28 × 0.07
Radiation	MoKα (λ = 0.71073)
2Θ range for data collection/°	5.77 to 61.012
Index ranges	-13 ≤ h ≤ 13, -15 ≤ k ≤ 15, -25 ≤ l ≤ 25
Reflections collected	21034
Independent reflections	9480 [R_{int} = 0.0183, R_{sigma} = 0.0251]
Data/restraints/parameters	9480/0/515
Goodness-of-fit on F^2	1.117
Final R indexes [I>=2σ (I)]	R_1 = 0.0253, wR_2 = 0.0626
Final R indexes [all data]	R_1 = 0.0267, wR_2 = 0.0636
Largest diff. peak/hole / e Å^{-3}	1.14/-1.13

Table S2. Bond Lengths for **[Ag-CF_3]$_3$•CH_2Cl_2**.

Atom	Atom	Length/Å	Atom	Atom	Length/Å
Ag1	N1	2.1162(14)	F25	C18	1.331(2)
Ag1	N6	2.1142(14)	F26	C18	1.329(2)
Ag2	N2	2.1199(15)	F27	C18	1.329(2)
Ag2	N3	2.1267(15)	N1	N2	1.3574(19)
Ag3	N4	2.1212(15)	N1	C1	1.341(2)
Ag3	N5	2.1156(14)	N2	C3	1.342(2)
F1	C4	1.337(2)	N3	N4	1.362(2)
F2	C4	1.340(2)	N3	C7	1.343(2)
F3	C4	1.330(2)	N4	C9	1.344(2)
F4	C5	1.336(2)	N5	N6	1.3584(19)
F5	C5	1.3356(19)	N5	C13	1.342(2)
F6	C5	1.342(2)	N6	C15	1.338(2)
F7	C6	1.344(2)	C1	C2	1.392(2)
F8	C6	1.339(2)	C1	C4	1.496(2)
F9	C6	1.333(2)	C2	C3	1.395(2)
F10	C10	1.337(2)	C2	C5	1.492(2)
F11	C10	1.328(2)	C3	C6	1.500(2)
F12	C10	1.344(2)	C7	C8	1.394(2)
F13	C11	1.332(2)	C7	C10	1.505(3)
F14	C11	1.340(2)	C8	C9	1.390(2)
F15	C11	1.331(2)	C8	C11	1.494(2)
F16	C12	1.341(2)	C9	C12	1.505(3)
F17	C12	1.325(2)	C13	C14	1.393(2)
F18	C12	1.335(2)	C13	C16	1.505(2)
F19	C16	1.329(2)	C14	C15	1.390(2)
F20	C16	1.340(2)	C14	C17	1.491(2)
F21	C16	1.337(2)	C15	C18	1.500(2)
F22	C17	1.344(2)	Cl1	C19	1.754(2)
F23	C17	1.330(2)	Cl2	C19	1.787(2)
F24	C17	1.340(2)			

Table S3. Bond Angles for **[Ag-CF_3]$_3$•**CH_2Cl_2**.

Atom	Atom	Atom	Angle/˚	Atom	Atom	Atom	Angle/˚
N6	Ag1	N1	167.87(6)	C9	C8	C7	103.73(15)
N2	Ag2	N3	174.98(6)	C9	C8	C11	128.04(17)
N5	Ag3	N4	176.13(6)	N4	C9	C8	110.20(16)
N2	N1	Ag1	120.82(11)	N4	C9	C12	120.64(16)
C1	N1	Ag1	131.01(11)	C8	C9	C12	129.16(15)
C1	N1	N2	108.15(13)	F10	C10	F12	107.25(16)
N1	N2	Ag2	117.70(10)	F10	C10	C7	111.73(15)
C3	N2	Ag2	134.15(12)	F11	C10	F10	106.96(16)
C3	N2	N1	108.04(14)	F11	C10	F12	107.24(15)
N4	N3	Ag2	121.37(11)	F11	C10	C7	112.78(15)
C7	N3	Ag2	130.62(13)	F12	C10	C7	110.59(15)
C7	N3	N4	107.91(14)	F13	C11	F14	106.87(17)
N3	N4	Ag3	121.83(11)	F13	C11	C8	111.95(16)
C9	N4	Ag3	130.08(12)	F14	C11	C8	112.21(16)
C9	N4	N3	108.00(14)	F15	C11	F13	106.89(17)
N6	N5	Ag3	117.03(10)	F15	C11	F14	106.77(17)
C13	N5	Ag3	135.02(11)	F15	C11	C8	111.79(16)
C13	N5	N6	107.95(13)	F16	C12	C9	110.84(15)
N5	N6	Ag1	121.96(11)	F17	C12	F16	107.16(15)
C15	N6	Ag1	129.82(11)	F17	C12	F18	106.77(17)
C15	N6	N5	108.00(13)	F17	C12	C9	112.75(15)
N1	C1	C2	110.12(15)	F18	C12	F16	107.33(16)
N1	C1	C4	120.29(15)	F18	C12	C9	111.70(15)
C2	C1	C4	129.52(15)	N5	C13	C14	110.14(14)
C1	C2	C3	103.64(14)	N5	C13	C16	120.52(15)
C1	C2	C5	127.81(15)	C14	C13	C16	129.29(15)
C3	C2	C5	128.54(15)	C13	C14	C17	129.58(15)
N2	C3	C2	110.06(14)	C15	C14	C13	103.53(14)

Table S3. Bond Angles for **[Ag-CF_3]$_3$•CH_2Cl_2**.

Atom	Atom	Atom	Angle/˚	Atom	Atom	Atom	Angle/˚
N2	C3	C6	121.05(15)	C15	C14	C17	126.89(15)
C2	C3	C6	128.88(15)	N6	C15	C14	110.38(14)
F1	C4	F2	107.07(15)	N6	C15	C18	119.51(15)
F1	C4	C1	111.58(14)	C14	C15	C18	130.11(15)
F2	C4	C1	111.29(15)	F19	C16	F20	107.70(16)
F3	C4	F1	107.33(15)	F19	C16	F21	106.85(15)
F3	C4	F2	107.16(15)	F19	C16	C13	111.58(14)
F3	C4	C1	112.13(14)	F20	C16	C13	111.09(15)
F4	C5	F5	107.24(15)	F21	C16	F20	106.93(15)
F4	C5	F6	106.28(14)	F21	C16	C13	112.41(15)
F4	C5	C2	112.11(14)	F22	C17	C14	111.13(15)
F5	C5	F6	106.98(14)	F23	C17	F22	107.70(16)
F5	C5	C2	112.78(14)	F23	C17	F24	106.77(15)
F6	C5	C2	111.07(14)	F23	C17	C14	113.28(15)
F7	C6	C3	111.00(16)	F24	C17	F22	105.89(16)
F8	C6	F7	107.02(15)	F24	C17	C14	111.66(14)
F8	C6	C3	112.56(16)	F25	C18	C15	111.94(15)
F9	C6	F7	107.46(17)	F26	C18	F25	108.32(17)
F9	C6	F8	107.02(17)	F26	C18	F27	106.97(16)
F9	C6	C3	111.49(15)	F26	C18	C15	111.50(15)
N3	C7	C8	110.16(16)	F27	C18	F25	106.13(15)
N3	C7	C10	120.71(16)	F27	C18	C15	111.68(15)
C8	C7	C10	129.11(16)	Cl1	C19	Cl2	111.67(11)
C7	C8	C11	128.21(17)				

Single crystal X-ray crystallography of $[Ag\text{-}CF_3\bullet(C_2H_4)]_2$

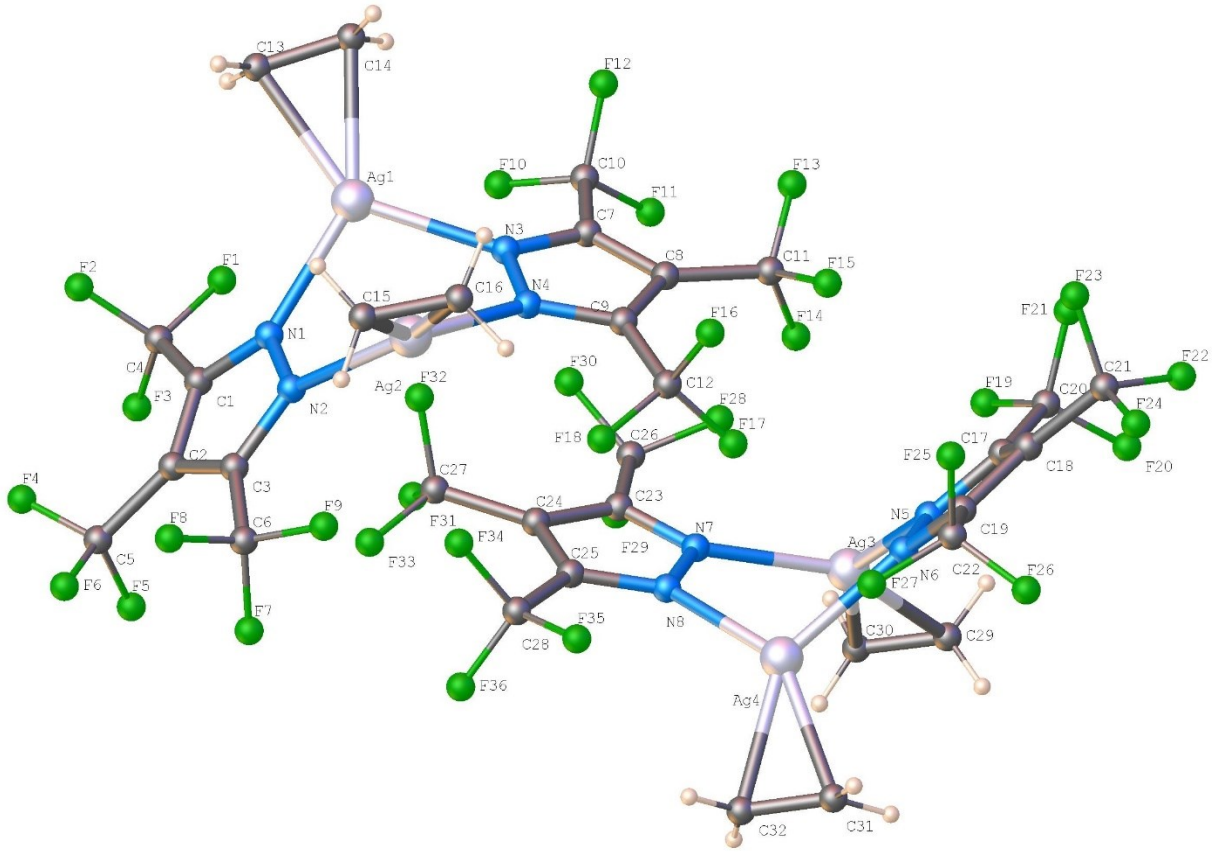

Figure S9. Molecular structure and atom labelling scheme of **$[Ag\text{-}CF_3\bullet(C_2H_4)]_2$.** There are two molecules in the asymmetric unit.

Table S4. Crystal data and structure refinement for **$[Ag\text{-}CF_3\bullet(C_2H_4)]_2$**.

Identification code	rad679a_b
Empirical formula	C16H8Ag2F18N4
Formula weight	814.00
Temperature/K	100.0
Crystal system	orthorhombic
Space group	$Pna2_1$
a/Å	18.4248(8)

b/Å	29.1743(13)
c/Å	8.8130(4)
α/°	90
β/°	90
γ/°	90
Volume/Å^3	4737.3(4)
Z	8
ρ_{calc}g/cm^3	2.283
μ/mm^{-1}	1.809
F(000)	3104.0
Crystal size/mm^3	0.35 × 0.12 × 0.08
Radiation	MoKα (λ = 0.71073)
2Θ range for data collection/°	5.836 to 61.128
Index ranges	-26 ≤ h ≤ 26, -41 ≤ k ≤ 41, -12 ≤ l ≤ 12
Reflections collected	64520
Independent reflections	14467 [Rint = 0.0339, Rsigma = 0.0281]
Data/restraints/parameters	14467/121/787
Goodness-of-fit on F^2	1.082
Final R indexes [I>=2σ (I)]	R1 = 0.0273, wR2 = 0.0601
Final R indexes [all data]	R1 = 0.0301, wR2 = 0.0610
Largest diff. peak/hole / e Å^{-3}	1.08/-0.80
Flack parameter	0.49(2)

Table S5. Bond Lengths for **[Ag-CF$_3$•(C$_2$H$_4$)]$_2$**.

Atom	Atom	Length/Å	Atom	Atom	Length/Å
Ag1	N1	2.223(4)	Ag3	N5	2.215(4)
Ag1	N3	2.231(3)	Ag3	N7	2.224(3)
Ag1	C13	2.287(5)	Ag3	C29	2.276(5)
Ag1	C14	2.272(5)	Ag3	C30	2.264(5)
Ag2	N2	2.242(4)	Ag4	N6	2.241(4)

Table S5. Bond Lengths for **[Ag-CF_3•(C_2H_4)]$_2$**.

Atom	Atom	Length/Å	Atom	Atom	Length/Å
Ag2	N4	2.235(3)	Ag4	N8	2.240(3)
Ag2	C15	2.287(5)	Ag4	C31	2.305(5)
Ag2	C16	2.281(5)	Ag4	C32	2.284(5)
F1	C4	1.332(6)	F19	C20	1.338(6)
F2	C4	1.327(6)	F20	C20	1.330(6)
F3	C4	1.320(6)	F21	C20	1.341(6)
F4	C5	1.334(6)	F22	C21	1.332(6)
F5	C5	1.331(7)	F23	C21	1.350(7)
F6	C5	1.330(6)	F24	C21	1.337(6)
F7	C6	1.332(6)	F25	C22	1.340(6)
F8	C6	1.338(5)	F26	C22	1.339(5)
F9	C6	1.342(6)	F27	C22	1.327(6)
F10	C10	1.334(5)	F28	C26	1.323(6)
F11	C10	1.336(5)	F29	C26	1.339(6)
F12	C10	1.332(5)	F30	C26	1.329(5)
F13	C11	1.334(6)	F31	C27	1.326(5)
F14	C11	1.321(7)	F32	C27	1.325(6)
F15	C11	1.338(7)	F33	C27	1.329(6)
F16	C12	1.332(7)	F34	C28	1.335(6)
F17	C12	1.319(6)	F35	C28	1.327(5)
F18	C12	1.330(6)	F36	C28	1.335(6)
N1	N2	1.353(5)	N5	N6	1.354(5)
N1	C1	1.335(6)	N5	C17	1.342(6)
N2	C3	1.336(6)	N6	C19	1.337(5)
N3	N4	1.355(4)	N7	N8	1.350(4)
N3	C7	1.334(5)	N7	C23	1.336(5)
N4	C9	1.340(5)	N8	C25	1.345(5)
C1	C2	1.393(6)	C17	C18	1.391(6)
C1	C4	1.496(6)	C17	C20	1.495(6)
C2	C3	1.390(6)	C18	C19	1.396(6)

Table S5. Bond Lengths for **[Ag-CF_3•(C_2H_4)]$_2$**.

Atom	Atom	Length/Å	Atom	Atom	Length/Å
C2	C5	1.490(7)	C18	C21	1.467(7)
C3	C6	1.485(6)	C19	C22	1.498(6)
C7	C8	1.387(6)	C23	C24	1.393(5)
C7	C10	1.494(6)	C23	C26	1.492(5)
C8	C9	1.387(6)	C24	C25	1.392(6)
C8	C11	1.492(6)	C24	C27	1.492(6)
C9	C12	1.494(6)	C25	C28	1.499(6)
C13	C14	1.359(7)	C29	C30	1.331(8)
C15	C16	1.349(8)	C31	C32	1.335(8)

Table S6. Bond Angles for **[Ag-CF_3•(C_2H_4)]$_2$**.

Atom	Atom	Atom	Angle/˚	Atom	Atom	Atom	Angle/˚
N1	Ag1	N3	102.23(13)	N5	Ag3	N7	101.50(14)
N1	Ag1	C13	113.44(17)	N5	Ag3	C29	112.46(17)
N1	Ag1	C14	148.00(16)	N5	Ag3	C30	146.45(17)
N3	Ag1	C13	144.06(18)	N7	Ag3	C29	145.57(19)
N3	Ag1	C14	109.40(17)	N7	Ag3	C30	111.60(18)
C14	Ag1	C13	34.69(19)	C30	Ag3	C29	34.1(2)
N2	Ag2	C15	113.14(18)	N6	Ag4	C31	109.83(18)
N2	Ag2	C16	147.35(17)	N6	Ag4	C32	143.63(17)
N4	Ag2	N2	101.25(13)	N8	Ag4	N6	103.16(14)
N4	Ag2	C15	144.88(19)	N8	Ag4	C31	146.0(2)
N4	Ag2	C16	111.36(17)	N8	Ag4	C32	112.75(19)
C16	Ag2	C15	34.3(2)	C32	Ag4	C31	33.8(2)
N2	N1	Ag1	119.0(3)	N6	N5	Ag3	117.7(3)
C1	N1	Ag1	133.3(3)	C17	N5	Ag3	134.1(3)
C1	N1	N2	107.7(4)	C17	N5	N6	108.2(3)
N1	N2	Ag2	118.3(3)	N5	N6	Ag4	117.6(3)

Table S6. Bond Angles for **[Ag-CF_3•(C_2H_4)]$_2$**.

Atom	Atom	Atom	Angle/˚	Atom	Atom	Atom	Angle/˚
C3	N2	Ag2	133.2(3)	C19	N6	Ag4	134.8(3)
C3	N2	N1	108.5(4)	C19	N6	N5	107.5(3)
N4	N3	Ag1	118.6(2)	N8	N7	Ag3	118.4(2)
C7	N3	Ag1	133.2(3)	C23	N7	Ag3	132.9(3)
C7	N3	N4	108.1(3)	C23	N7	N8	108.5(3)
N3	N4	Ag2	118.6(2)	N7	N8	Ag4	116.8(2)
C9	N4	Ag2	133.3(3)	C25	N8	Ag4	135.7(3)
C9	N4	N3	107.8(3)	C25	N8	N7	107.6(3)
N1	C1	C2	110.5(4)	N5	C17	C18	110.5(4)
N1	C1	C4	120.0(4)	N5	C17	C20	119.8(4)
C2	C1	C4	129.5(4)	C18	C17	C20	129.7(4)
C1	C2	C5	128.8(4)	C17	C18	C19	102.7(4)
C3	C2	C1	103.3(4)	C17	C18	C21	128.3(4)
C3	C2	C5	127.9(4)	C19	C18	C21	129.1(4)
N2	C3	C2	110.0(4)	N6	C19	C18	111.0(4)
N2	C3	C6	120.6(4)	N6	C19	C22	119.8(4)
C2	C3	C6	129.4(4)	C18	C19	C22	129.2(4)
F1	C4	C1	111.7(4)	F19	C20	F21	106.5(4)
F2	C4	F1	106.3(4)	F19	C20	C17	111.7(4)
F2	C4	C1	112.4(4)	F20	C20	F19	106.6(4)
F3	C4	F1	106.4(4)	F20	C20	F21	107.2(4)
F3	C4	F2	107.4(4)	F20	C20	C17	112.8(4)
F3	C4	C1	112.3(4)	F21	C20	C17	111.7(4)
F4	C5	C2	111.9(4)	F22	C21	F23	105.4(5)
F5	C5	F4	106.0(5)	F22	C21	F24	107.1(5)
F5	C5	C2	112.9(4)	F22	C21	C18	112.8(4)
F6	C5	F4	106.9(4)	F23	C21	C18	113.1(4)
F6	C5	F5	107.1(5)	F24	C21	F23	105.4(5)
F6	C5	C2	111.7(4)	F24	C21	C18	112.4(4)

Table S6. Bond Angles for **[Ag-CF_3•(C_2H_4)]$_2$**.

Atom	Atom	Atom	Angle/˚	Atom	Atom	Atom	Angle/˚
F7	C6	F8	107.1(4)	F25	C22	C19	111.3(4)
F7	C6	F9	106.8(4)	F26	C22	F25	106.4(4)
F7	C6	C3	112.1(4)	F26	C22	C19	112.4(4)
F8	C6	F9	106.0(4)	F27	C22	F25	106.4(4)
F8	C6	C3	112.6(4)	F27	C22	F26	106.9(4)
F9	C6	C3	111.9(4)	F27	C22	C19	113.0(4)
N3	C7	C8	110.3(4)	N7	C23	C24	110.3(3)
N3	C7	C10	120.1(4)	N7	C23	C26	119.7(3)
C8	C7	C10	129.5(4)	C24	C23	C26	130.0(4)
C7	C8	C11	127.7(4)	C23	C24	C27	128.1(4)
C9	C8	C7	103.6(4)	C25	C24	C23	103.1(3)
C9	C8	C11	128.7(4)	C25	C24	C27	128.9(4)
N4	C9	C8	110.2(3)	N8	C25	C24	110.5(3)
N4	C9	C12	119.6(4)	N8	C25	C28	120.2(4)
C8	C9	C12	130.2(4)	C24	C25	C28	129.2(4)
F10	C10	F11	106.8(4)	F28	C26	F29	106.9(4)
F10	C10	C7	112.3(4)	F28	C26	F30	107.3(4)
F11	C10	C7	111.3(4)	F28	C26	C23	111.6(4)
F12	C10	F10	107.0(4)	F29	C26	C23	112.4(4)
F12	C10	F11	106.5(4)	F30	C26	F29	106.9(4)
F12	C10	C7	112.7(4)	F30	C26	C23	111.6(4)
F13	C11	F15	106.4(5)	F31	C27	F33	106.6(4)
F13	C11	C8	111.2(4)	F31	C27	C24	112.3(4)
F14	C11	F13	106.4(4)	F32	C27	F31	106.1(4)
F14	C11	F15	106.9(4)	F32	C27	F33	106.8(4)
F14	C11	C8	114.0(5)	F32	C27	C24	112.7(4)
F15	C11	C8	111.4(4)	F33	C27	C24	111.9(4)
F16	C12	C9	112.4(4)	F34	C28	F36	106.8(4)
F17	C12	F16	107.4(4)	F34	C28	C25	111.6(4)

Table S6. Bond Angles for **[Ag-CF_3•(C_2H_4)]$_2$**.

Atom	Atom	Atom	Angle/˚	Atom	Atom	Atom	Angle/˚
F17	C12	F18	107.1(4)	F35	C28	F34	106.9(4)
F17	C12	C9	112.0(4)	F35	C28	F36	107.3(4)
F18	C12	F16	105.6(4)	F35	C28	C25	111.7(4)
F18	C12	C9	111.9(4)	F36	C28	C25	112.2(4)
C14	C13	Ag1	72.1(3)	C30	C29	Ag3	72.4(3)
C13	C14	Ag1	73.2(3)	C29	C30	Ag3	73.5(3)
C16	C15	Ag2	72.6(3)	C32	C31	Ag4	72.3(3)
C15	C16	Ag2	73.1(3)	C31	C32	Ag4	73.9(3)

In situ synchrotron powder diffraction data collection (PXRD)

In situ powder x-ray diffraction data (PXRD) from solid samples in ethylene or helium were collected using the monochromatic X-rays available at the Advanced Photon Source, Argonne National Laboratory, beamline 17-BM. We used a circular incident beam (300 μm diameter) with ~0.45 Å wavelength for experiments in conjunction with a VAREX 4343 amorphous-Si flat panel detector. Samples of were loaded into 1.0 mm quartz capillaries with glass wool on either side. The capillary with sample was then loaded into a gas flow cell,[6] to perform in situ PXRD experiments. At one end the gas cell was connected to a two-way valve which allowed changing between a 1 atm helium flow and a high-pressure syringe pump (Teledyne ISCO 500D) which was filled with ethene gas. Pressure was monitored at the other end of the gas flow cell to make sure that there was no blockage or leak during the measurements. Pressures quoted are absolute, so a purge of helium or ethylene is a pressure of 1 bar. Prior to measurements, all samples were activated with supercritical ethylene (295 K, 55 bar) as described.[7]

Data Processing

The raw images were processed within GSAS-II,[8] refining the sample-to-detector distance and tilt of the detector relative to the beam based on data obtained for a LaB_6 standard.[9] Collected 2D detector images from *in situ* powder diffraction data sets were reduced to 1D datasets of intensity *vs.* diffraction angle 2θ with GSAS-II. Plots such as Figure S1, showing the evolution of the PXRD data were prepared with the same software, in which the diffracted intensity is represented by a color scale. In call cases, time runs from the bottom to the top of the image. Individual scans

were analyzed using Topas-Academic software.[10] Structures from powder data were determined by simulated annealing, using the single crystal structures as a starting point. The pyrazole groups were incorporated as rigid bodies based on the average geometries from analogous single crystal data, with the CF_3 rotations freely refined. Selected bond distances, angles, and torsions were refined as appropriate. The unexpected structure of **[Ag-H•(C_2H_4)]$_3$** was initially hypothesized from the volume of the indexed unit cell and was solved by repeated cycles of model building and refinement.

CIF files (PXRD based and from *in situ* synthesis) of previously unknown dinuclear **[Ag-Br•(C_2H_4)]$_2$** and trinuclear **[Ag-H•(C_2H_4)]$_3$** silver-ethylene complexes, along with the trinuclear precursor **[Ag-CF_3]$_3$** for which a single crystal was not available (for the latter, single crystal data have CH_2Cl_2 as solvents of crystallization), have been deposited at the Cambridge Crystallographic Data Centre with CCDC numbers 2267047, 2266818, and 2266816 respectively.

Table S7 summarizes the crystal structures of all of the unsolvated silver pyrazolates discussed in this work.

Table S7. Selected crystal data for materials discussed in this paper.

Compound	**[Ag-Br]$_3$**	**[Ag-Br•(C_2H_4)]$_2$**	**[Ag-H]$_3$**	**[Ag-H]$_3$**	**[Ag-H•(C_2H_4)]$_3$**	**[Ag-CF_3]$_3$**	**[Ag-CF_3•(C_2H_4)]$_2$**
Method	Single Crystal	Powder	Single Crystal	Single Crystal	Powder	Powder	Single Crystal
CCDC deposition	PIVJUB	2267047	XELXER	DAZGIV	2266818	2266816	2256900
Temperature / K	100	173	293	100	173	295	100
Atmosphere		10 bar C_2H_4			10 bar C_2H_4	He flow	
Formula	$C_{15}Ag_3Br_3F_{18}N_6$	$C_{15}H_8Ag_2Br_2F_{12}N_4$	$C_{15}H_3Ag_3F_{18}N_6$	$C_{15}H_3Ag_3F_{18}N_6$	$C21H_{15}Ag_3F_{18}N_6$	$C_{18}Ag_3F_{27}N_6$	$C_{16}H_8Ag_2F_{18}N_4$
Formula Wt	1169.5	835.8	932.8	932.8	1017.0	1136.8	814.0
Space Group	*Pbca*	$C222_1$	*C*2/*c*	*P* –1	*C*2/*c*	*P* –1	$Pna2_1$
a / Å	15.3955	14.1527	23.078	10.1597	12.9987	10.3875	18.4248
b / Å	14.0979	18.3542	13.4835	10.5111	13.4064	10.7481	29.1743
c / Å	23.9071	17.8705	23.773	11.6798	17.8789	13.9603	8.813
α (deg)	90	90	90	74.034	90	76.5993	90
β (deg)	90	90	97.014	74.724	97.4355	72.7054	90
γ (deg)	90	90	90	78.434	90	85.8995	90
Cell Volume (Å^3)	5188.9	4642.1	7342.1	1145.7	3089.5	1447.6	4737.3
Vol / molecule (Å^3)	648.6	580.3	611.8	572.9	772.4	723.8	592.2
Z / Z'	8 / 1	8 / 1	12 / 1.5	2 / 1	4 / 0.5	2 / 1	8 / 2
$R_{Profile}$ (%)		2.25			0.39	1.26	
R_{Bragg} (%)	3.13	2.53	3.68	2.81	0.49	0.75	3.01

In situ Powder X-ray Diffraction Studies of $[Ag\text{-}CF_3]_3$

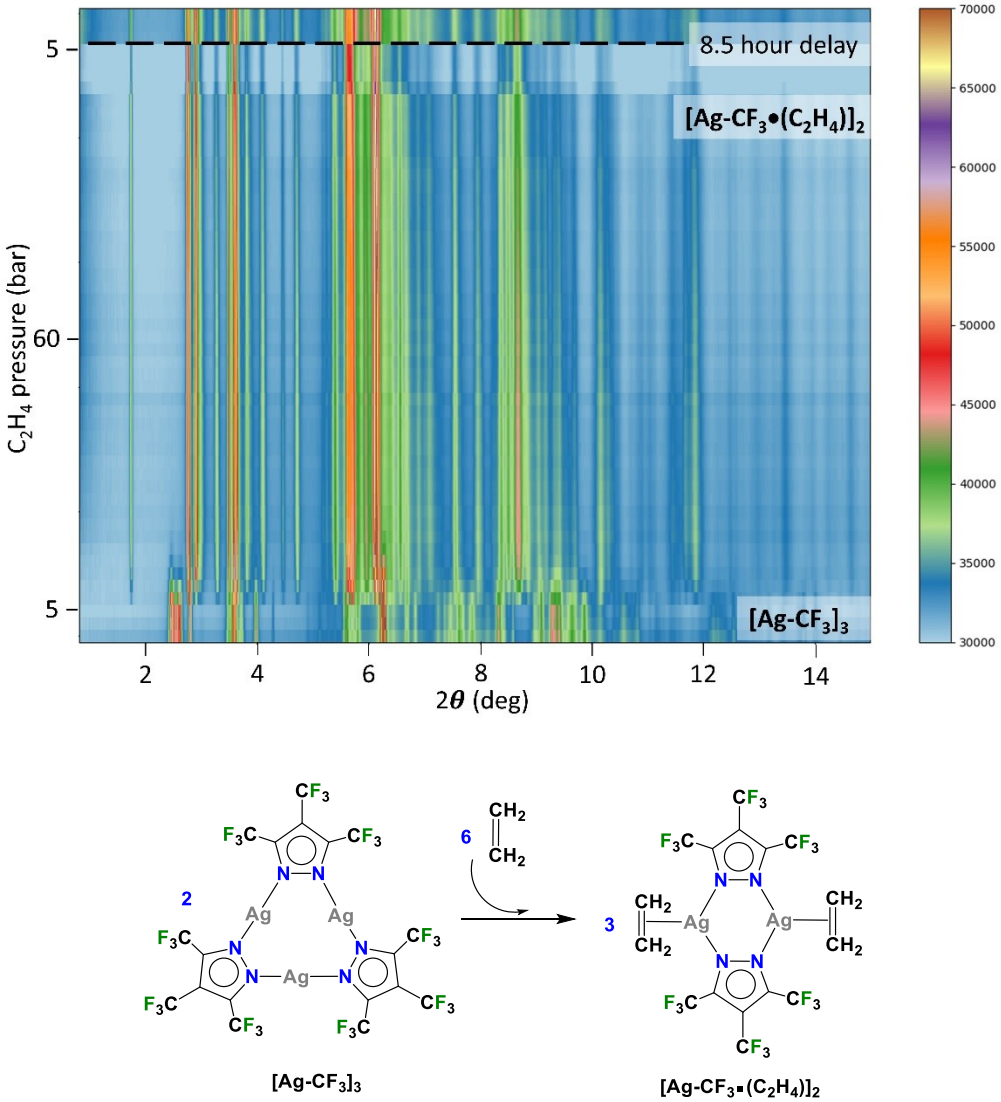

Figure S10. Conversion of **$[Ag\text{-}CF_3]_3$** to **$[Ag\text{-}CF_3\bullet(C_2H_4)]_2$** occurs at 3-5 bar at 295 K as evident from this experiment from 5-60-5 bar of ethylene at 295 K. This also shows that the reverse reaction does not take place at 295K under ethylene. Other experiments, not presented here, show that there is no solid-state reaction of ethylene with the unloaded trimer at 1 bar of ethylene flow at room temperature. Intensity scale (color bar on right) is in arbitrary units. The first scan, at bottom, was taken under He flow. Its trace, with Rietveld refinement, is shown in Figure S14.

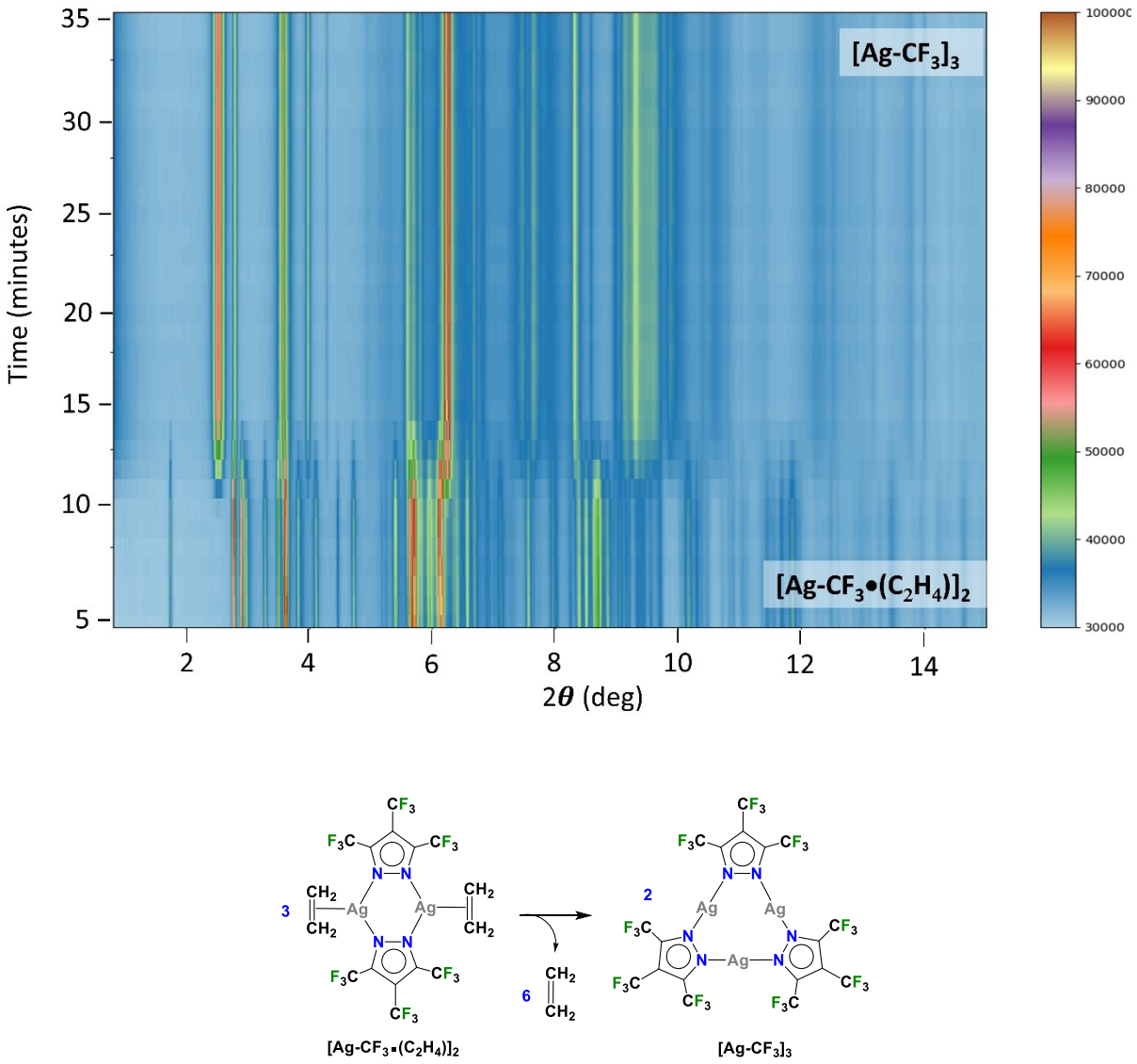

Figure S11. The **[Ag-CF₃•(C₂H₄)]₂** to **[Ag-CF₃]₃** conversion (the ethylene loss) under helium flow (~ 1 bar) at 295 K. Intensity scale (color bar on right) is in arbitrary units. The first scan, at bottom, is shown in Fig. S15, with Rietveld fit.

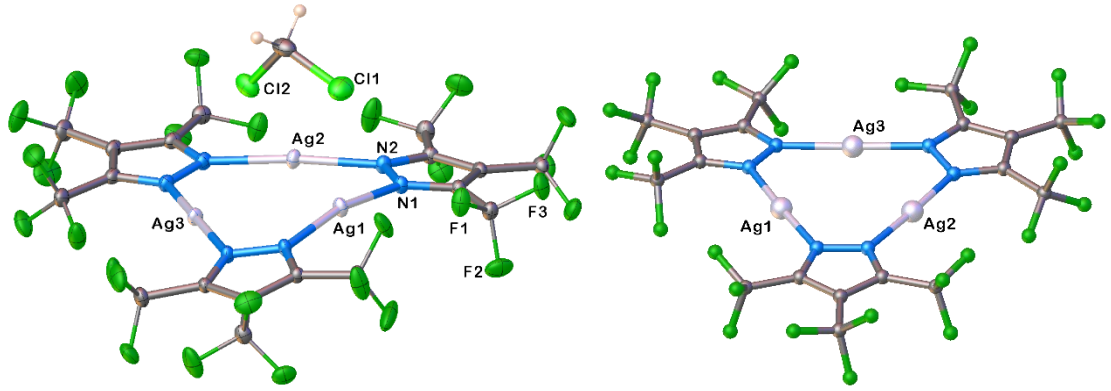

Figure S12. Single crystal X-ray structure of **[Ag-CF_3]$_3$**•CH_2Cl_2 (on left) and powder X-ray diffraction structure of **[Ag-CF_3]$_3$** (on right).

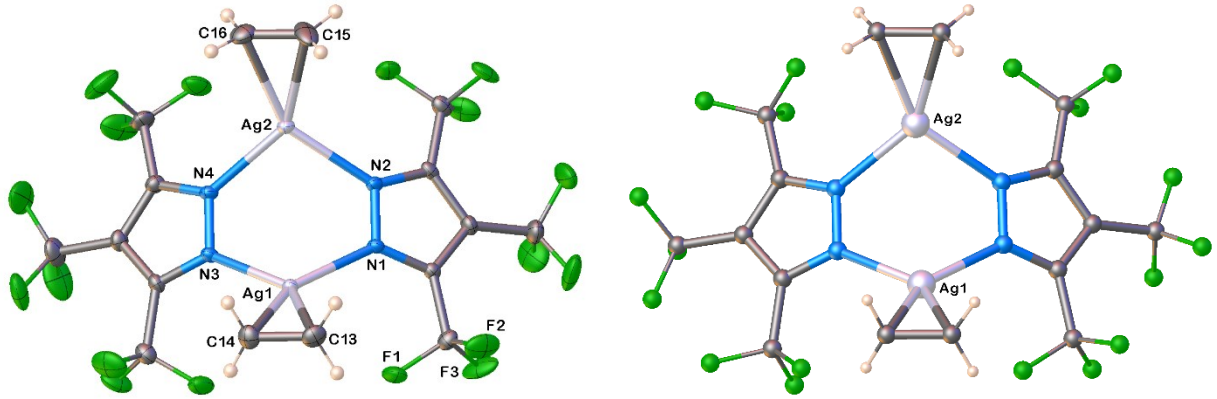

Figure S13. Molecular structure of **[Ag-CF_3•(C_2H_4)]$_2$** obtained from solution (left – using single crystal X-ray diffraction studies) and solid-state chemistry (right – from powder X-ray diffraction).

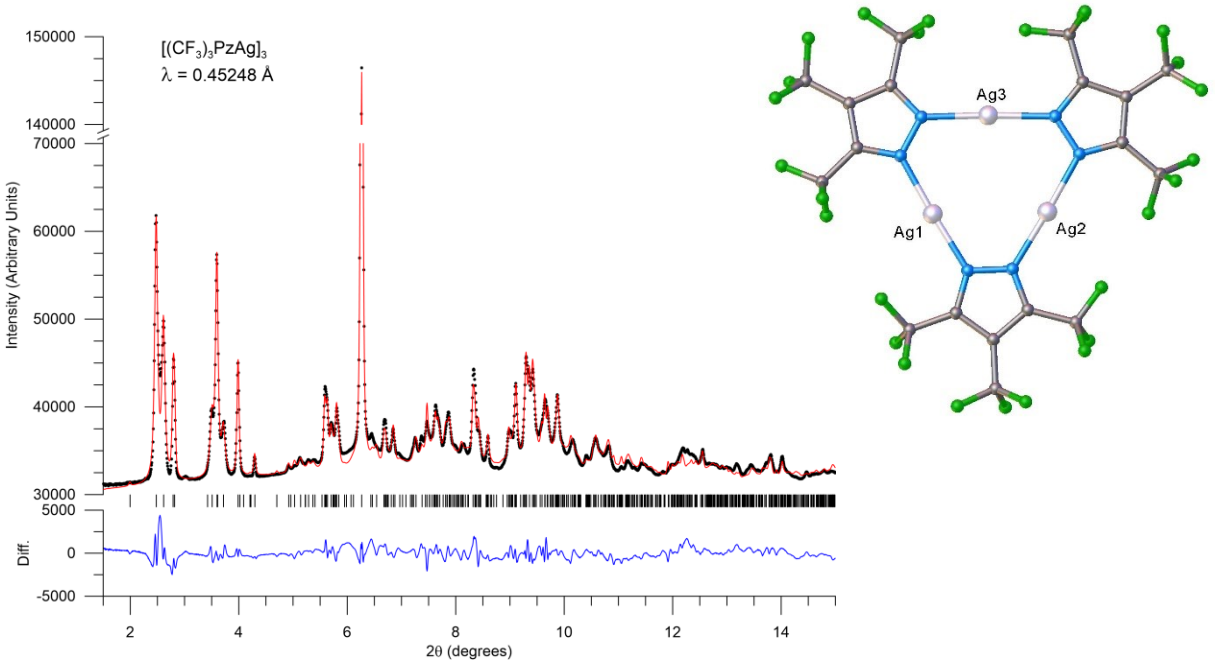

Figure S14. Rietveld fit of **[Ag-CF_3]$_3$.** This is the first data set shown at the bottom of Fig. S10, and is essentially identical to the data at the top of S11. Refined structure is illustrated on right. CCDC deposition 2266816.

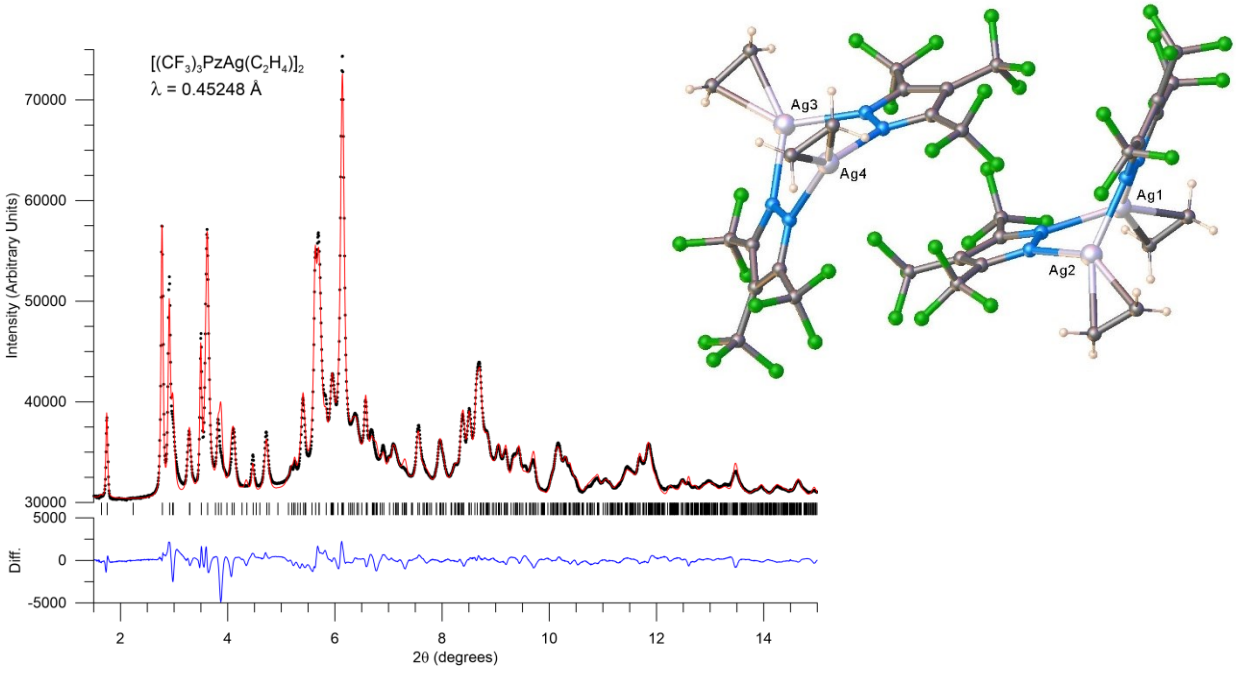

Figure S15. Rietveld fit of **[Ag-CF_3•(C_2H_4)]$_2$**, from the first data set at the bottom of Fig. S11. Refined structure on right. CCDC deposition 2266817

In situ Powder X-ray Diffraction Studies of $[Ag\text{-}H]_3$

$[Ag\text{-}H]_3$ reaction with pressure of C_2H_4 60bar 295K(*AgH3_C2H4_60bar*)

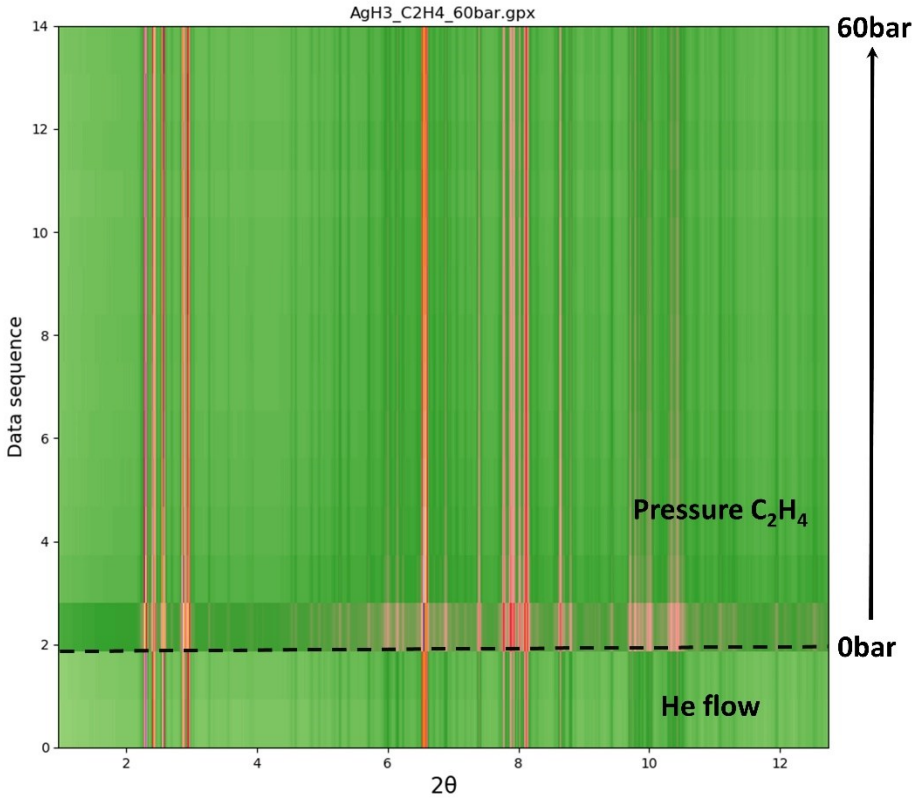

Figure S16. Evolution of the in situ PXRD patterns showing of ethylene and solid **$[Ag\text{-}H]_3$** reaction at 295 K with increasing ethylene pressure. No reaction was observed even at 60 bar.

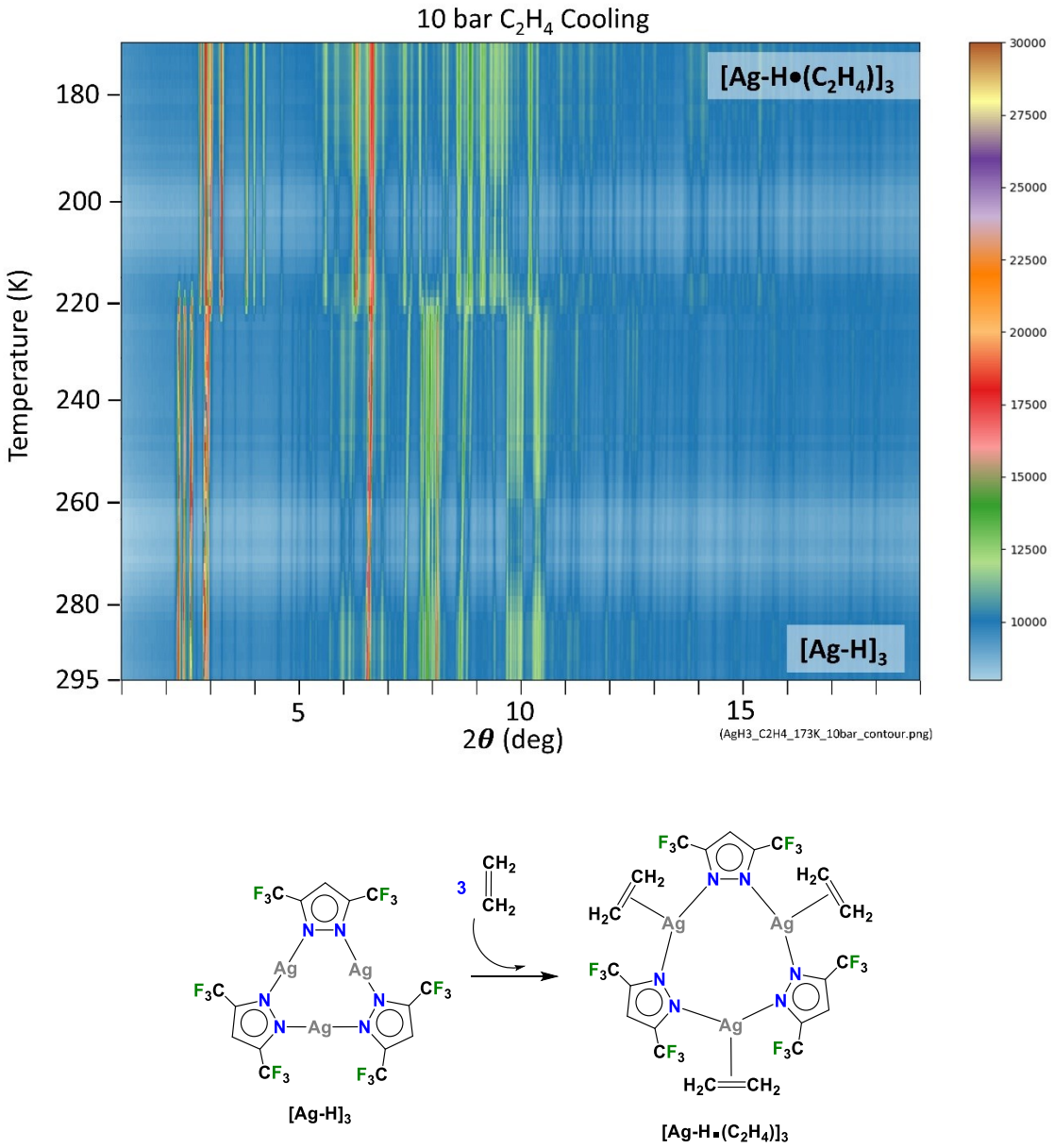

Figure S17. Evolution of the in situ PXRD patterns showing of ethylene and solid **[Ag-H]$_3$** reaction at **10 bar ethylene** with decreasing temperature. Formation of a new phase confirmed as {[3,5-$(CF_3)_2$Pz]Ag(C_2H_4)}$_3$ (**[Ag-H•(C_2H_4)]$_3$**) was observed starting at 223K. Intensity scale (color bar on right) is in arbitrary units.

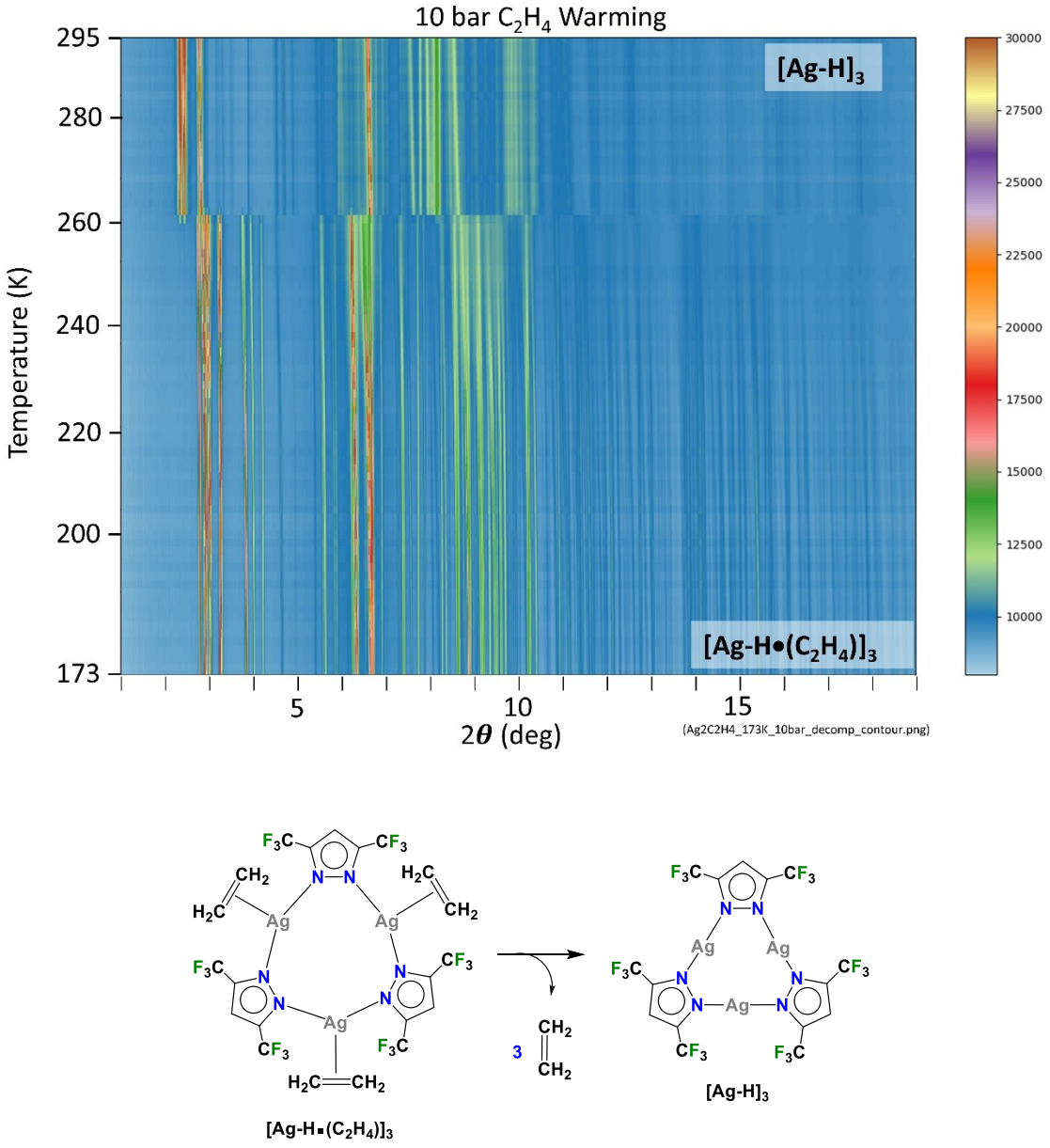

Figure S18. Evolution of the in situ PXRD patterns showing decomposition of {[3,5-$(CF_3)_2$Pz]Ag(C_2H_4)}$_3$ (**[Ag-H•(C_2H_4)]$_3$**) to produce ethylene free starting phase **[Ag-H]$_3$** at 10 bar ethylene with increasing temperature. Conversion to **[Ag-H]$_3$** was observed at 262K. Intensity scale (color bar on right) is in arbitrary units.

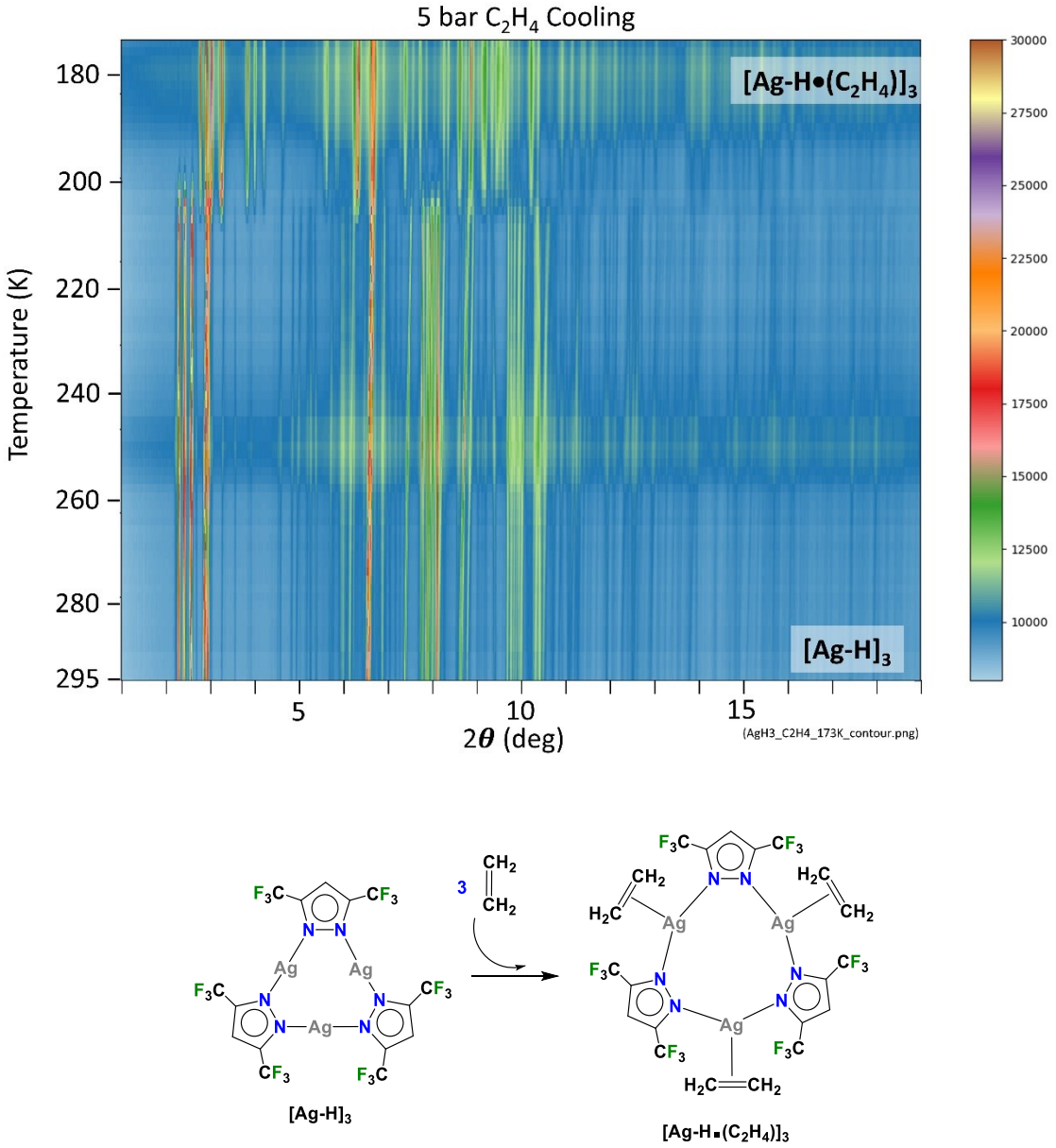

Figure S19. Evolution of the in situ PXRD patterns showing of ethylene and solid **[Ag-H]$_3$** reaction at **5 bar ethylene** with decreasing temperature. Formation of a new phase was observed starting 206K. It was confirmed as {[3,5-$(CF_3)_2$Pz]Ag(C_2H_4)}$_3$ (**[Ag-H•(C_2H_4)]$_3$**). Intensity scale (color bar on right) is in arbitrary units.

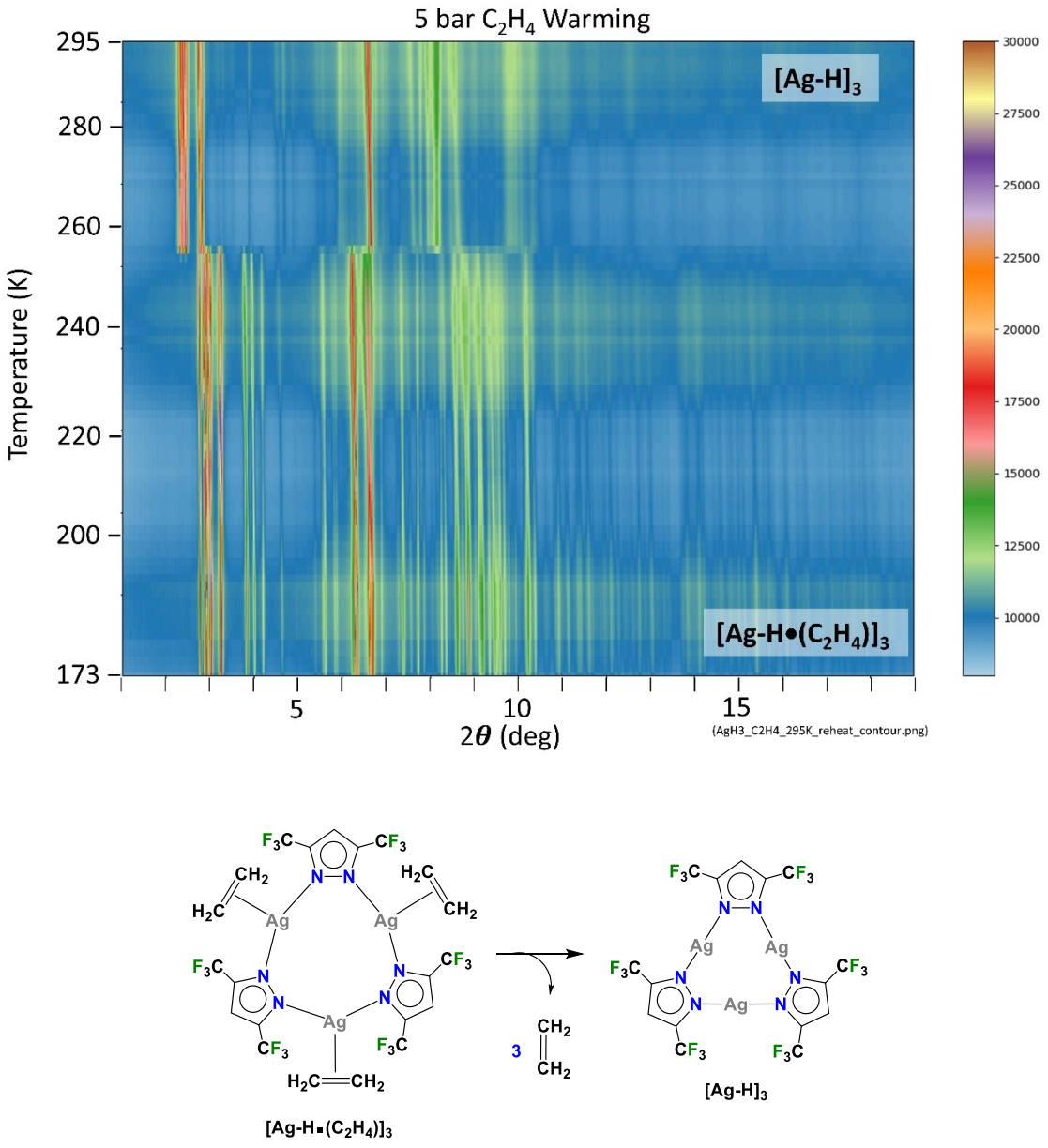

Figure S20. Evolution of the in situ PXRD patterns showing decomposition of {[3,5-$(CF_3)_2$Pz]Ag(C_2H_4)}$_3$ (**[Ag-H•(C_2H_4)]$_3$**) to produce ethylene free starting phase **[Ag-H]$_3$** at 5 bar ethylene with increasing temperature. Conversion to **[Ag-H]$_3$** was observed at 256K.

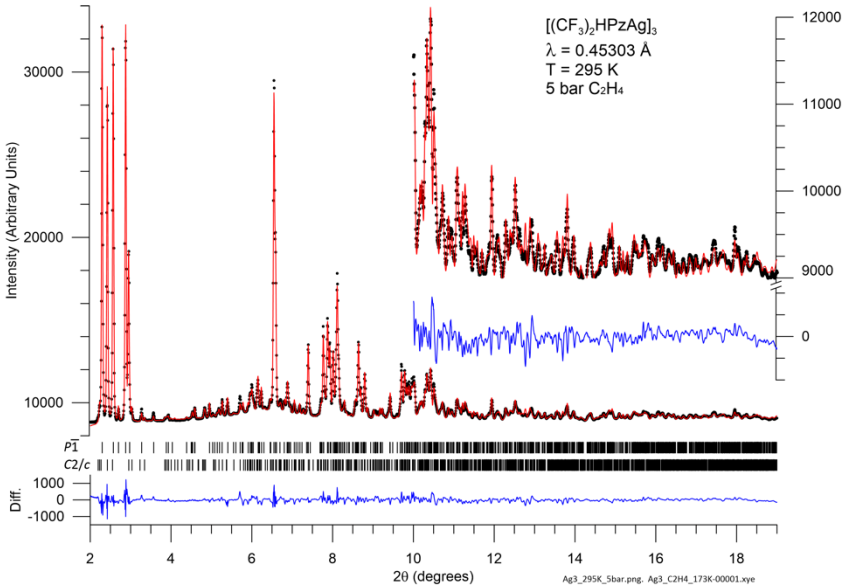

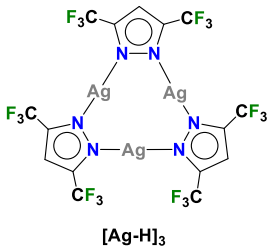

Figure S21. Rietveld fit of **[Ag-H]$_3$**, from the first scan shown at the bottom of Fig. S17. This sample is a mixture of the two crystal structures (i.e., polymorphs) of this compound, confirmed by comparisons to single crystal XRD. They are CCDC refcode DAZGIV (spacegroup P-1) 69%,[11] XELXER (spacegroup C2/c) 31%.[12]

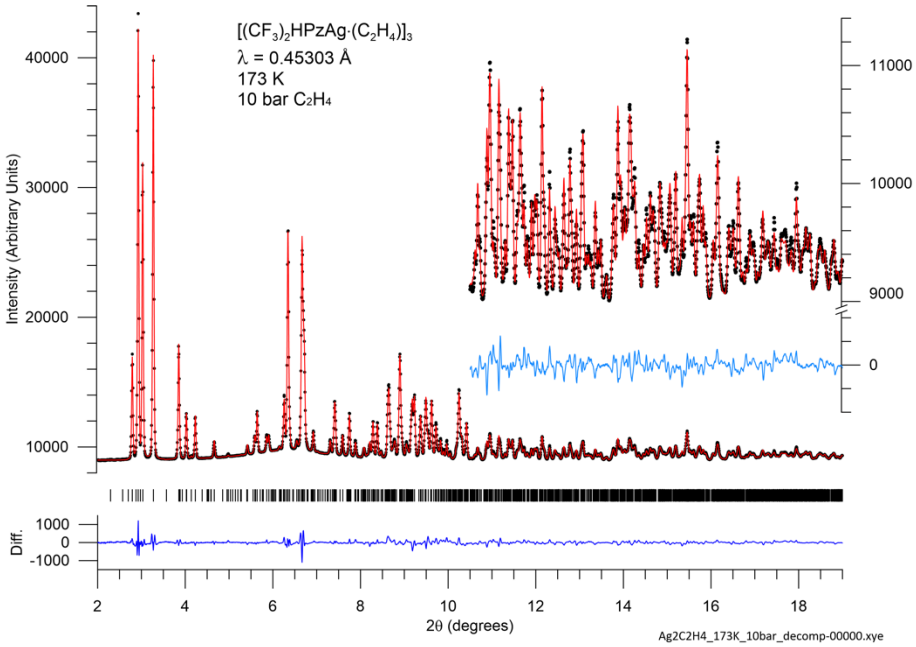

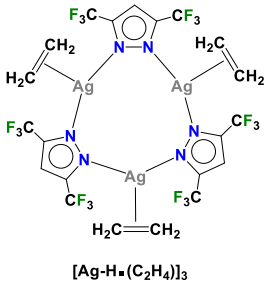

Figure S22. Rietveld fit of **[Ag-H•(C_2H_4)]$_3$**, shown at bottom of panel Fig. S18. CCDC deposition 2266818.

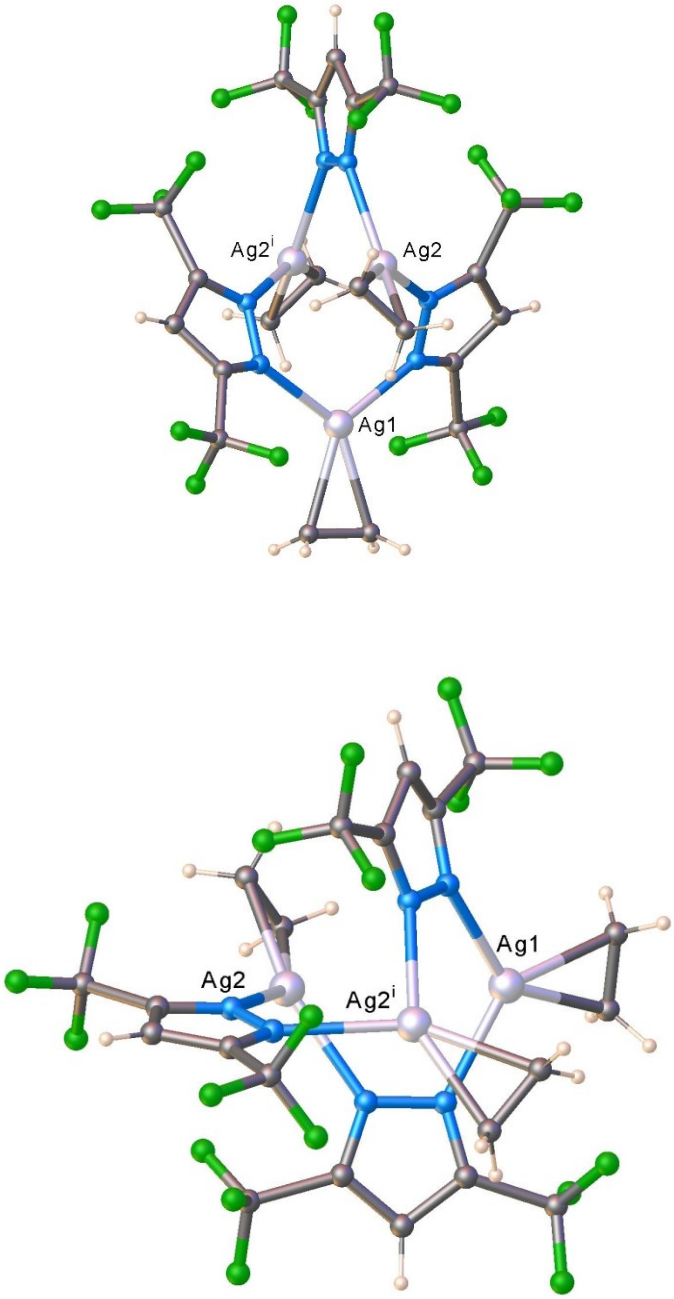

Figure S23. Two views of **[Ag-H•(C_2H_4)]$_3$** molecular structure, determined from powder diffraction data. CCDC deposition 2266818.

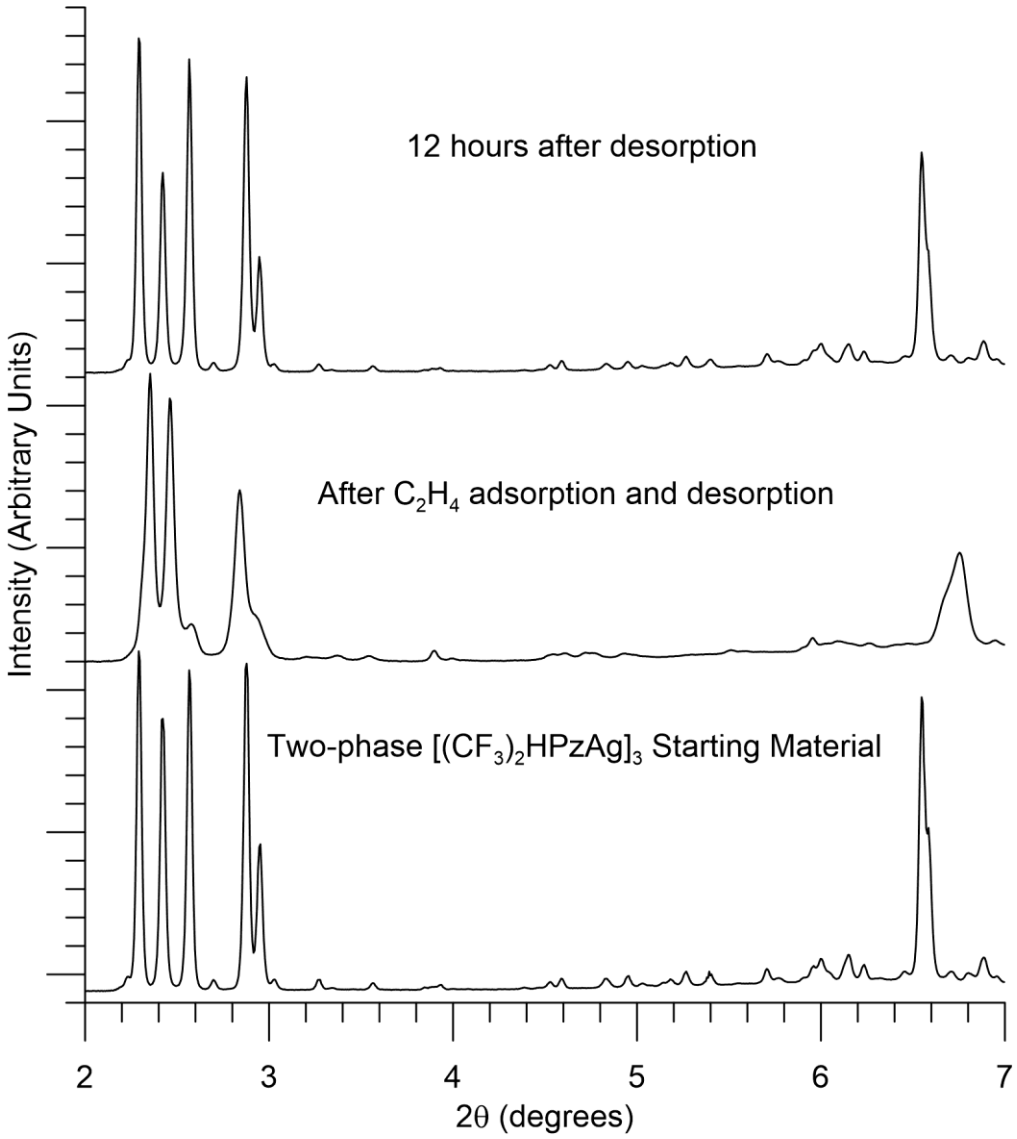

Figure S24. This shows evolution from the two-phase **[Ag-H]$_3$** starting material in the bottom panel, to a disordered **[Ag-H]$_3$** trimer phase (generated after ethylene uptake and removal cycle) in the middle panel. After 12 hours, the sample has settled into a clean mixture of the original two phases (see Figure S17 for information on different phases/polymorphs).

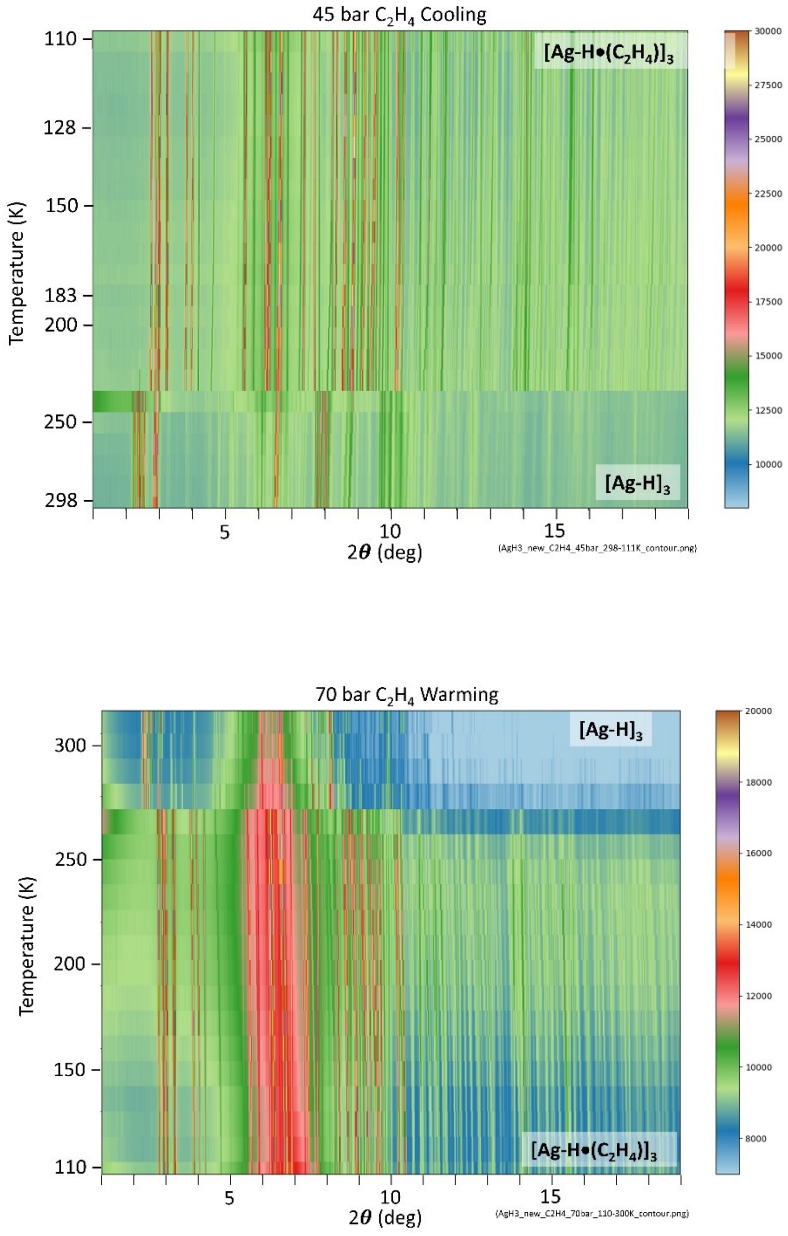

Figure S25. In search of **[Ag-H•(C_2H_4)]$_2$** (transition of ethylene bound silver trimer to expected ethylene bound silver dimer) under extreme conditions**. Top: [Ag-H]$_3$** from room temperature to 110K at 45 bar of ethylene, **Bottom:** Warming **[Ag-H•(C_2H_4)]$_3$** while maintaining very high ethylene pressure of 70 bar. In both cases no signs of a new phase (potentially **[Ag-H•(C_2H_4)]$_2$**) were observed. Warming leads to ethylene loss and **[Ag-H]$_3$** formation, even under high ethylene pressure.

In situ Powder X-ray Diffraction Studies of $[Ag\text{-}Br]_3$

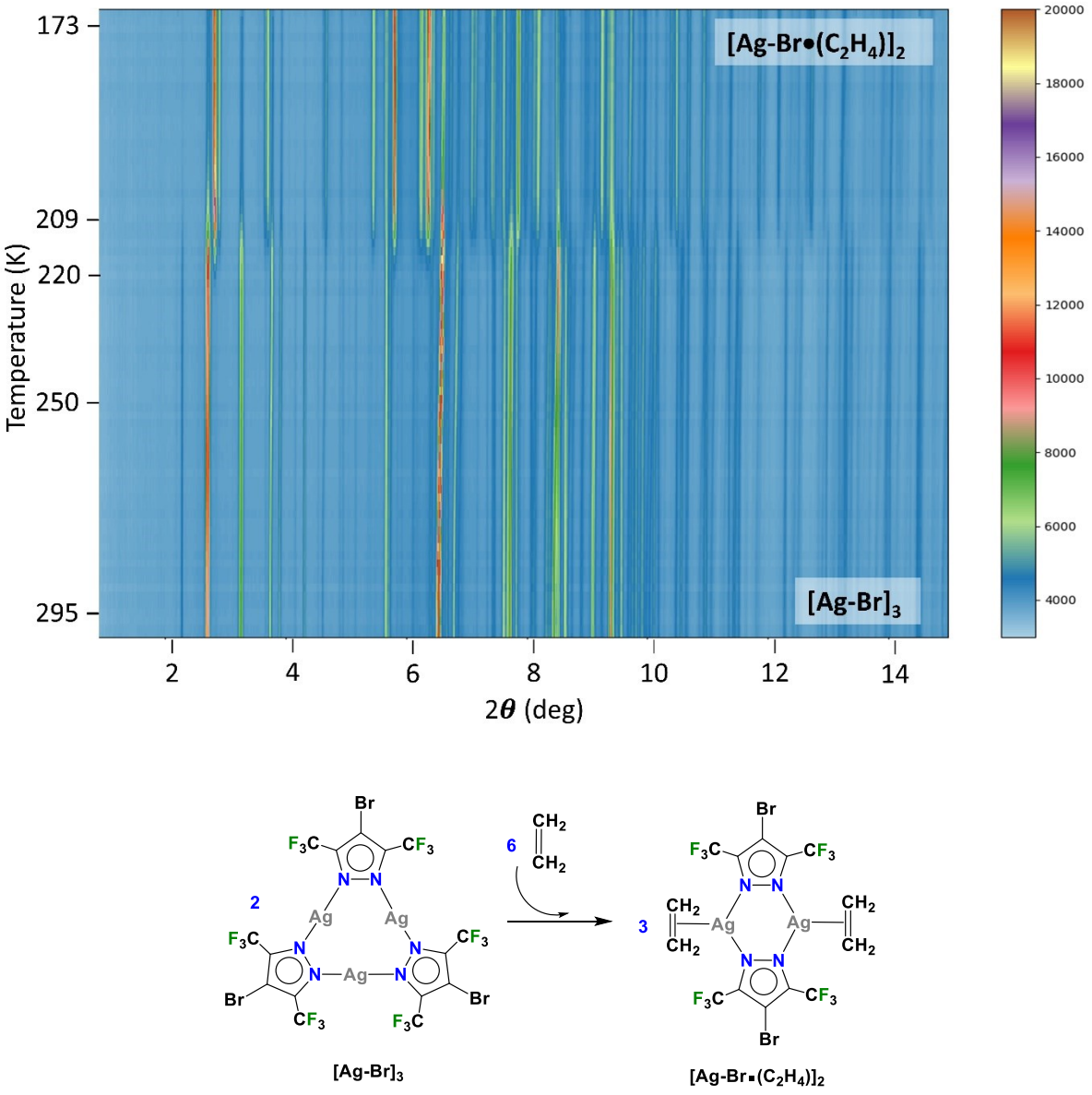

Figure S26. Evolution of the in situ PXRD patterns showing of ethylene and solid **$[Ag\text{-}Br]_3$** reaction at 10 bar ethylene with decreasing temperature. Formation of a new phase confirmed as $\{[4\text{-Br-3,5-}(CF_3)_2Pz]Ag(C_2H_4)\}_2$ (**$[Ag\text{-}Br\bullet(C_2H_4)]_2$**) was observed starting 220K through Rietveld fit shown in Fig. S29. Intensity scale (color bar on right) is in arbitrary units.

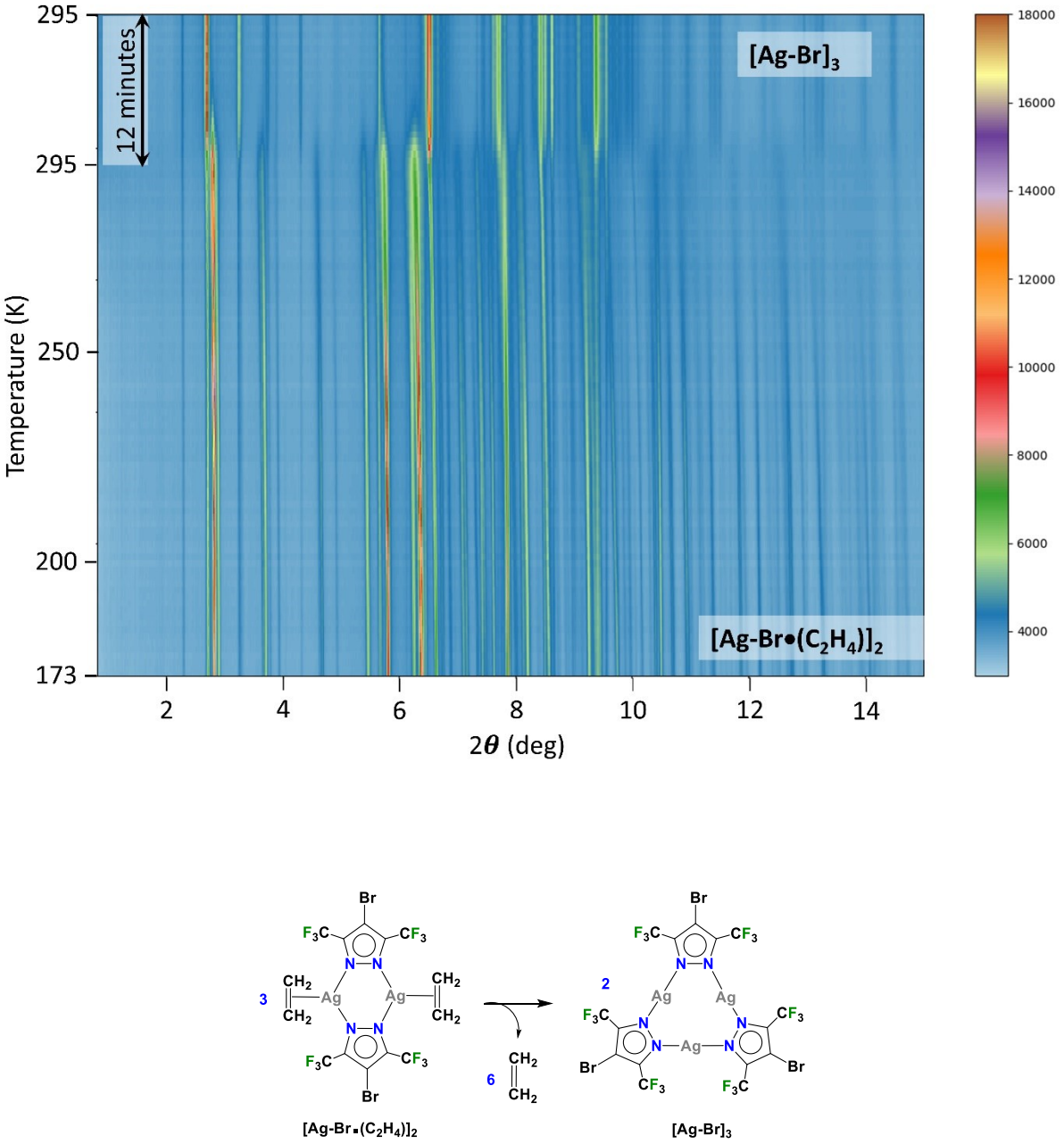

Figure S27. Evolution of the in situ PXRD patterns showing decomposition of {[4-Br-3,5-$(CF_3)_2$Pz]Ag(C_2H_4)}$_2$ (**[Ag-Br•(C_2H_4)]$_2$**) to produce ethylene free starting phase **[Ag-Br]$_3$** at 10 bar ethylene with increasing temperature. Conversion to **[Ag-Br]$_3$** was observed at 295K (which was slow at 295K and 10 bar ethylene). Single crystal XRD structure of **[Ag-Br]$_3$** (crystallized from solutions) has been reported and has CCDC refcode PIVJUB.[13]

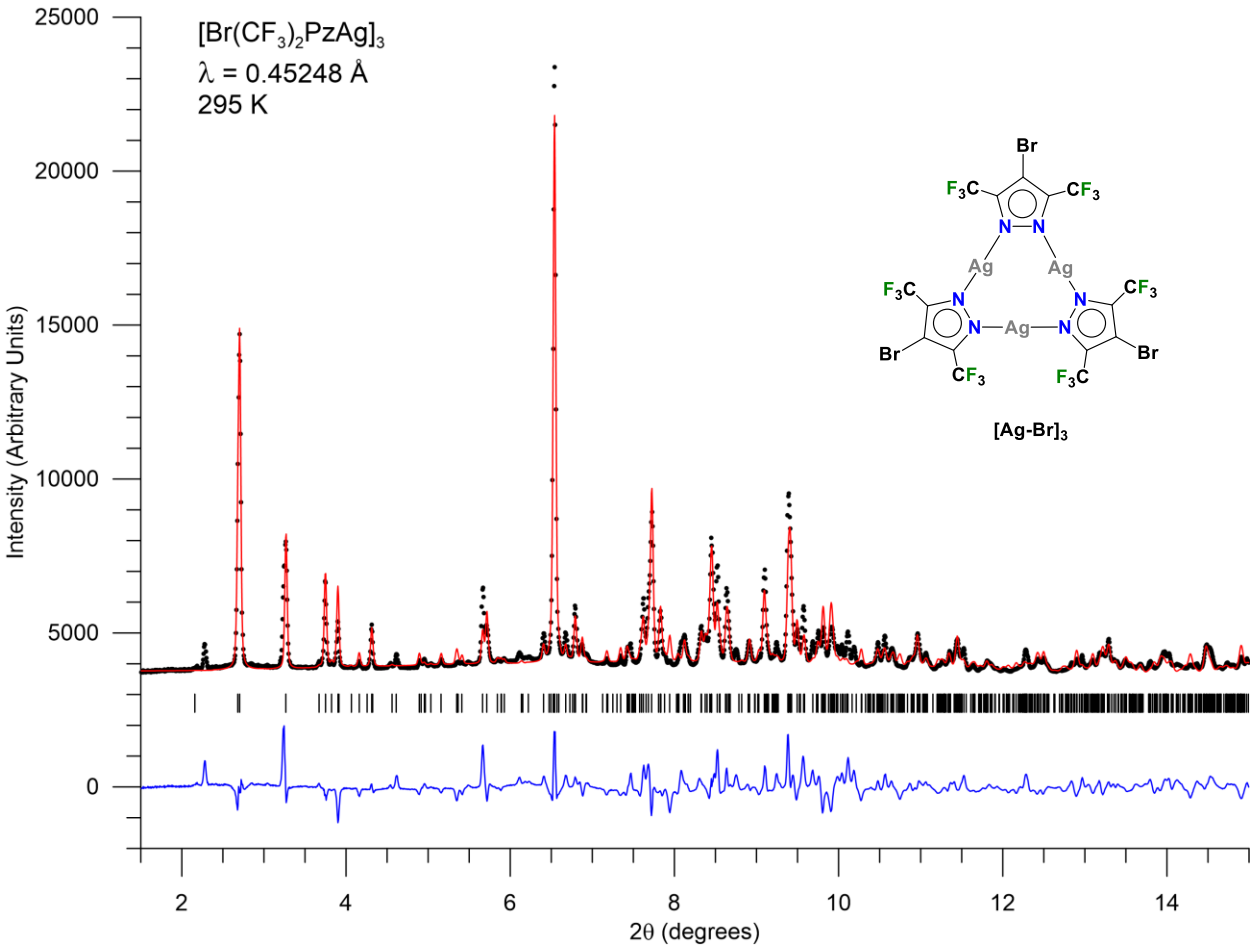

Figure S28. Rietveld of **[Ag-Br]$_3$** starting material, with several unidentified impurity peaks. Lattice parameters and position and orientation of molecule in unit cell were refined. This is the first (lowest) scan of contour plot of **[Ag-Br]$_3$** → **[Ag-Br•(C_2H_4)]$_2$** in Figure S26. Single crystal XRD structure of **[Ag-Br]$_3$** (crystallized from solutions) has been reported and has CCDC refcode PIVJUB.[13]

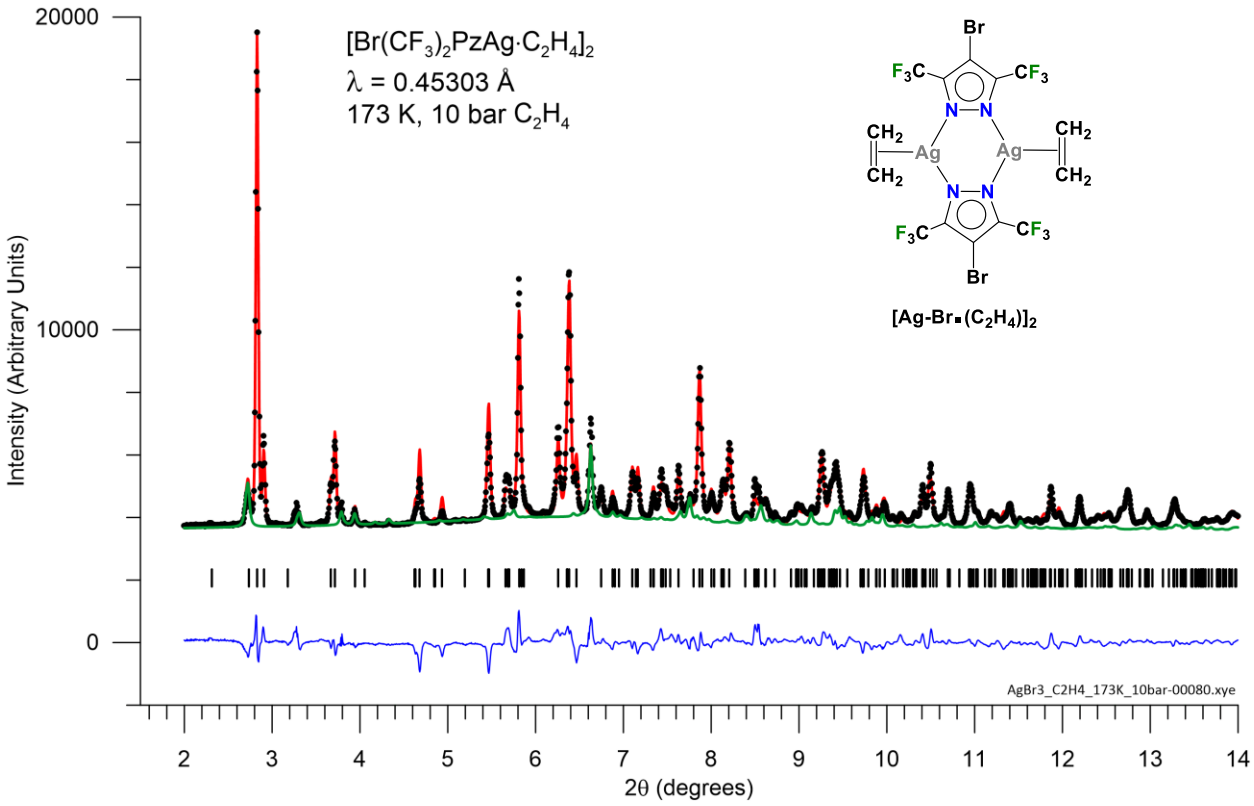

Figure S29. Rietveld of **[Ag-Br•(C_2H_4)]$_2$**. Reaction is incomplete with ~15% **[Ag-Br]$_3$** starting material left as shown in green trace. This is the last (top) scan of contour plot of **[Ag-Br]$_3$** → **[Ag-Br•(C_2H_4)]$_2$** in Figure S26. CCDC deposition 2267047.

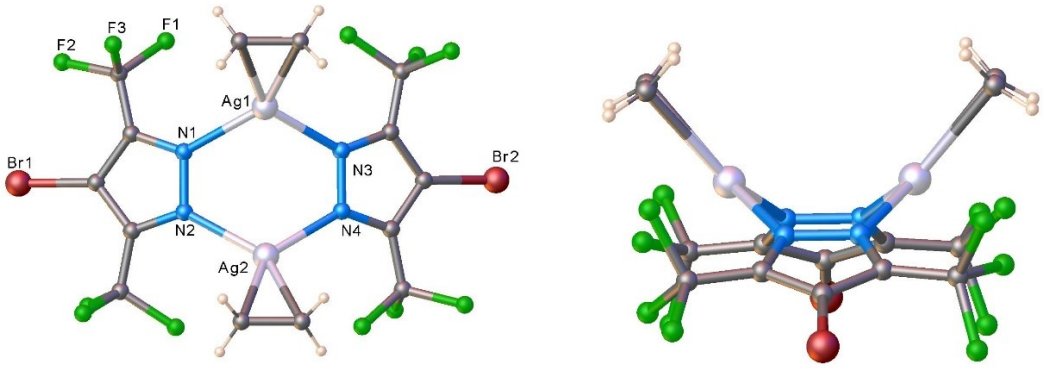

Figure S30. Two views of molecular structure of **[Ag-Br•(C_2H_4)]$_2$** based on above in situ powder X-ray diffraction data.

Computational studies and results

All calculations were carried out by using relativistic DFT methods employing the ADF code[14] with the all-electron triple-ζ Slater basis set plus the double-polarization (STO-TZ2P) basis set in conjunction with the Becke-Perdew (BP86) functional[15] within the generalized gradient approximation (GGA). London dispersion corrections were taken into account via the pair-wise Grimme3 approach.[16] Such level of theory is denoted as TZ2P/BP86-D3. Geometry optimizations were performed without any symmetry restrain, via the analytical energy gradient method implemented by Versluis and Ziegler,[17] with energy convergence criteria set at 10^{-4} Hartree, gradient convergence criteria at 10^{-4} Hartree/Å and radial convergence of 10^{-3} Å. Thermodynamic properties were obtained from vibrational analysis. Scalar relativistic effects were considered through the ZORA Hamiltonian.[17]

The interaction energy is further dissected into several chemically meaningful terms according to the Energy Decomposition Analysis (EDA) of Ziegler and Rauk,[18]

$\Delta E_{int} = \Delta E_{Pauli} + \Delta E_{elstat} + \Delta E_{orb} + \Delta E_{disp}$

where ΔE_{Pauli} term involves the electron repulsion between occupied orbitals from the different fragments. ΔE_{elstat} and ΔE_{orb} are related to the stabilizing electrostatic and covalent character of the interaction, respectively. The contribution from dispersion interaction (ΔE_{disp}) is evaluated using the pairwise correction of Grimme (D3).

Table S8. Difference in energy between planar and puckered Ag_3N_6 conformation of **[Ag-H]$_3$**, **[Ag-Br]$_3$**, and **[Ag-CF$_3$]$_3$**, in the absence of ethylene. Values given in kcal/mol.

[Ag-CF$_3$]$_3$	46.31
[Ag-Br]$_3$	49.44
[Ag-H]$_3$	50.52

Table S9. Interaction energy for the Ag_2N_4-AgN_2 interaction and related energy decomposition analysis at intermediate **2** structures (see Figure S31), in order to account for the release of a AgN_2 unit.

	[Ag-CF$_3$]$_3$		**[Ag-Br]$_3$**		**[Ag-H]$_3$**	
ΔE_{Pauli}	116.1		115.6		137.2	
ΔE_{Elstat}	-110.1	61.0%	-107.4	59.4%	-137.1	62.0%
ΔE_{Orb}	-42.4	23.5%	-45.1	24.9%	-56.6	25.6%
ΔE_{Disp}	-28.0	15.5%	-28.3	15.7%	-27.4	12.4%
ΔE_{Int}	-64.3		-65.2		-83.8	

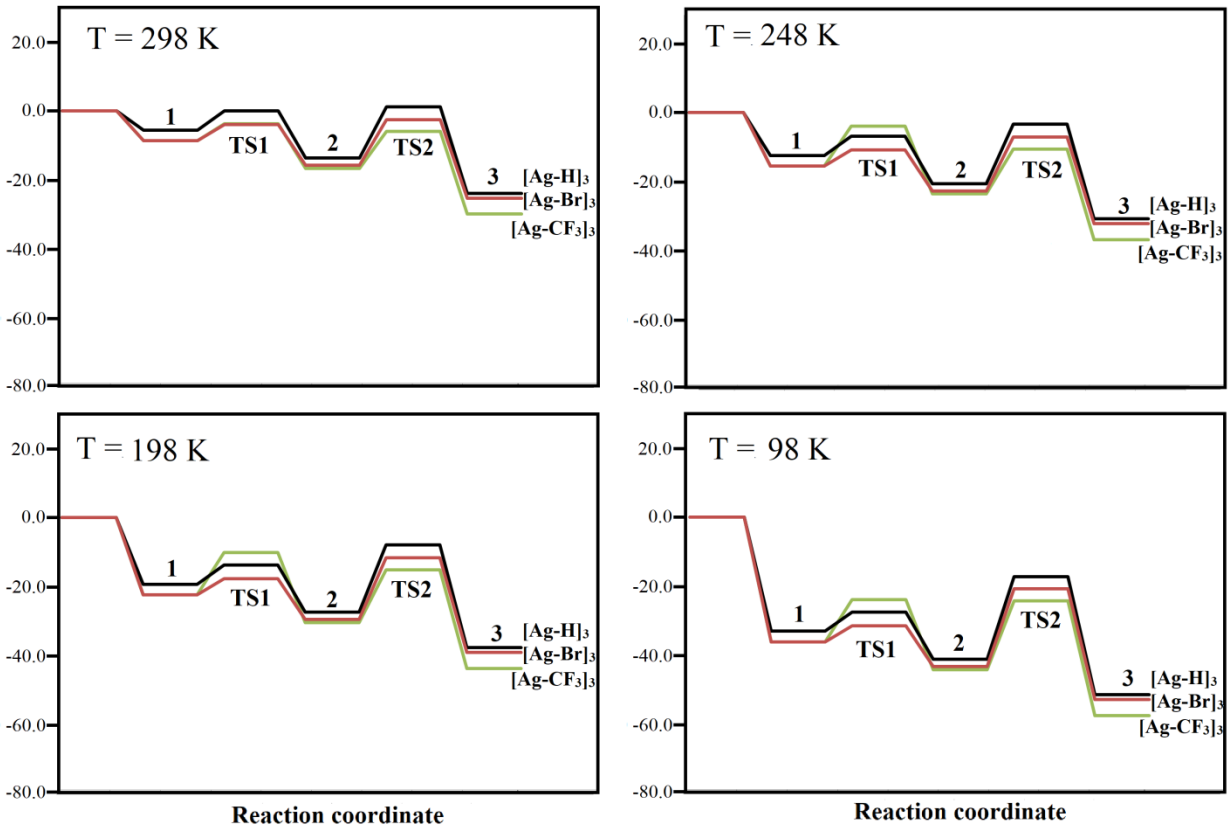

Figure S31. Graphical representation of Gibbs free energy difference for reaction coordinates at different temperatures. Values in kcal/mol, see Table S9.

Table S10. Gibbs free energy difference for reaction coordinates at different temperatures. Values in kcal/mol.

T = 298 K	**1**	**TS1**	**2**	**TS2**	**3**
$[Ag\text{-}CF_3]_3$	-8.7	-3.7	-16.8	-6.0	-30.1
$[Ag\text{-}Br]_3$	-8.7	-4.0	-15.9	-2.5	-25.5
$[Ag\text{-}H]_3$	-5.6	0.0	-13.7	1.2	-24.1
T = 248 K					
$[Ag\text{-}CF_3]_3$	-15.6	-3.9	-23.7	-10.6	-37.1
$[Ag\text{-}Br]_3$	-15.6	-10.9	-22.8	-7.1	-32.4
$[Ag\text{-}H]_3$	-12.5	-6.9	-20.7	-3.4	-31.0
T = 198 K					
$[Ag\text{-}CF_3]_3$	-22.5	-10.2	-30.6	-15.2	-44.0
$[Ag\text{-}Br]_3$	-22.5	-17.8	-29.7	-11.7	-39.3
$[Ag\text{-}H]_3$	-19.4	-13.8	-27.6	-8.0	-37.9
T = 98 K					
$[Ag\text{-}CF_3]_3$	-36.3	-24.0	-44.4	-24.4	-57.8
$[Ag\text{-}Br]_3$	-36.3	-31.7	-43.5	-20.9	-53.1
$[Ag\text{-}H]_3$	-33.2	-27.7	-41.4	-17.3	-51.7

References:

[1] E. Y. Slobodyanyuk, O. S. Artamonov, O. V. Shishkin, P. K. Mykhailiuk, *Eur. J. Org. Chem.* **2014**, *2014*, 2487-2495.

[2] L. Krause, R. Herbst-Irmer, G. M. Sheldrick, D. Stalke, *J. Appl. Crystallogr.* **2015**, *48*, 3-10.

[3] G. M. Sheldrick, *Acta Crystallogr. A, Found. Adv.* **2015**, *71*, 3-8.

[4] G. M. Sheldrick, *Acta Crystallogr. C, Struct. Chem.* **2015**, *71*, 3-8.

[5] O. V. Dolomanov, L. J. Bourhis, R. J. Gildea, J. A. K. Howard, H. Puschmann, *J. Appl. Crystallogr.* **2009**, *42*, 339-341.

[6] P. J. Chupas, K. W. Chapman, C. Kurtz, J. C. Hanson, P. L. Lee, C. P. Grey, *J. Appl. Crystallogr.* **2008**, *41*, 822-824.

[7] D. Parasar, A. H. Elashkar, A. A. Yakovenko, N. B. Jayaratna, B. L. Edwards, S. G. Telfer, H. V. R. Dias, M. G. Cowan, *Angewandte Chemie, International Edition* **2020**, *59*, 21001-21006.

[8] B. H. Toby, R. B. Von Dreele, *J. Appl. Crystallogr.* **2013**, *46*, 544-549.

[9] A. Hammersley, S. Svensson, M. Hanfland, A. Fitch, D. Hausermann, *High Press. Res.* **1996**, *14*, 235-248.

[10] A. A. Coelho, Topas Version 7 Technical Reference, **2020**. http:/www. topas-academic.net

[11] M. A. Omary, M. A. Rawashdeh-Omary, M. W. A. Gonser, O. Elbjeirami, T. Grimes, T. R. Cundari, H. V. K. Diyabalanage, C. S. P. Gamage, H. V. R. Dias, *Inorg. Chem.* **2005**, *44*, 8200-8210.

[12] H. V. R. Dias, S. A. Polach, Z. Wang, *J. Fluor. Chem.* **2000**, *103*, 163-169.

[13] C. V. Hettiarachchi, M. A. Rawashdeh-Omary, D. Korir, J. Kohistani, M. Yousufuddin, H. V. R. Dias, *Inorg. Chem.* **2013**, *52*, 13576-13583.

[14] S. ADF 2019, Theoretical Chemistry, Vrije Universiteit, Amsterdam, The Netherlands, p. http://www.scm.com.

[15] A. D. Becke, *Phys. Rev. A* **1988**, *38*, 3098-3100.

[16] S. Grimme, *WIREs Computational Molecular Science* **2011**, *1*, 211-228.

[17] L. Versluis, T. Ziegler, *J. Chem. Phys.* **1988**, *88*, 322-328.

[18] T. Ziegler, A. Rauk, *Inorg. Chem.* **1979**, *18*, 1558-1565.